Physics in Medicine & Biology

IPEM Institute of Physics and Engineering in Medicine

ACCEPTED MANUSCRIPT

Assessing cardiac stiffness using ultrasound shear wave elastography

To cite this article before publication: Annette Caenen *et al* 2021 *Phys. Med. Biol.* in press https://doi.org/10.1088/1361-6560/ac404d

Assessing cardiac stiffness using ultrasound shear wave elastography

Annette Caenen[a,b,c], Mathieu Pernot[d], Kathryn R. Nightingale[e], Jens-Uwe Voigt[b,f], Hendrik J. Vos[c], Patrick Segers[a*], Jan D'hooge[b*]

[a]*Institute for Biomedical Engineering and Technology, Ghent University, Ghent, Belgium.*

[b]*Department of Cardiovascular Sciences, University of Leuven, KU Leuven, Leuven, Belgium.*

[c]*Department of Cardiology, Erasmus MC University Medical Center, Rotterdam, the Netherlands.*

[d]*Physics for Medicine, INSERM, CNRS, ESPCI, PSL University, Paris, France.*

[e]*Department of Biomedical Engineering, Duke University, Durham (NC), United States.*

[f]*Department of Cardiovascular Diseases, University Hospital Leuven, KU Leuven, Leuven, Belgium.*

**Joint last author.*

Address for correspondence:

Annette Caenen, Institute for Biomedical Engineering and Technology, Ghent University, Campus Heymans - Blok B, Corneel Heymanslaan 10, 9000 Gent, Belgium. Phone: +32 9 332 02 58. Email: annette.caenen@ugent.be

Abstract

Shear wave elastography offers a new dimension to echocardiography: it measures myocardial stiffness. Therefore, it could provide additional insights into the pathophysiology of cardiac diseases affecting myocardial stiffness and potentially improve diagnosis or guide patient treatment. The technique detects fast mechanical waves on the heart wall with high frame rate echography, and converts their propagation speed into a stiffness value. A proper interpretation of shear wave data is required as the shear wave interacts with the intrinsic, yet dynamically changing geometrical and material characteristics of the heart under pressure. This dramatically alters the wave physics of the propagating wave, demanding adapted processing methods compared to other shear wave elastography applications as breast tumor and liver stiffness staging. Furthermore, several advanced analysis methods have been proposed to extract supplementary material features such as viscosity and anisotropy, potentially offering additional diagnostic value. This review explains the general mechanical concepts underlying cardiac shear wave elastography and provides an overview of the preclinical and clinical studies within the field. We also identify the mechanical and technical challenges ahead to make shear wave elastography a valuable tool for clinical practice.

Abbreviations

2D	Two-dimensional
3D	Three-dimensional
AK	Atrial kick
AP3C	Apical three-chamber view
AP4C	Apical four-chamber view
ARF	Acoustic radiation force
AVC	Aortic valve closure
ECG	Echocardiogram
ED	End-diastolic
EDP	End-diastolic pressure
ESP	End-systolic pressure
FA	Fractional anisotropy
FFT	Fast Fourier transform
HCM	Hypertrophic cardiomyopathy
HT	Hypertension
HTX	Heart transplantation
HV	Healthy volunteer
IVS	Interventricular septum
LAD	Left anterior descending coronary artery
LCX	Left circumflex coronary artery
LV	Left ventricle
LVFW	Left ventricular free wall
MI	Myocardial infarction
MS	Mechanical stimulation
MVC	Mitral valve closure
PLAX	Parasternal long axis view
PSAX	Parasternal short axis view
SWE	Shear wave elastography
TOF	Time-of-flight
US	Ultrasound
VC	Valve closure

Introduction

Echocardiographic evaluation of cardiac function is indispensable for the diagnosis and treatment of any cardiovascular disease. For many years, various indices based on measures of ventricular geometry and/or velocity measurements of blood flow and tissue have been proposed for the assessment of systolic or diastolic function, but none of these allow for a complete description of cardiac function. Indeed, cardiac distensibility and contractility – two important determinants of cardiac function – are tightly intertwined with active and passive myocardial stiffness, which is intrinsically linked with alterations at the level of the cardiomyocytes, crossbridge actin-myosin interactions and the composition of the extracellular matrix. Non-invasive ultrasound based evaluation of tissue stiffness started in the late 1980s to early 1990s, when a field based on the old technique of palpation was founded: ultrasound (US) elastography (Ophir *et al.*, 1991; Gao *et al.*, 1996). Later, around 2010, the advent of high-frame rate imaging meant a dogma shift for medical US: the entire field of view was insonified for every transmit in order to enable image reconstruction on receive at high frame rates (> 500 frames/s) in contrast to the conventional line-by-line scanning. This high frame rate imaging modality enabled new methodologies in elastography (Villemain *et al.*, 2020). In this review, we focus on one specific class of high frame rate techniques within the field of ultrasound elastography, referred to as shear wave elastography (SWE). Other imaging fields such as magnetic resonance imaging have developed similar technologies and we refer the reader interested in magnetic resonance elastography to literature on the topic, e.g. (Elgeti and Sack, 2014).

SWE – as the name suggests – uses the propagation characteristics of shear waves to estimate the stiffness of the tissue in which they propagate. Shear waves are naturally induced in the heart upon closure of atrio-ventricular or ventriculo-arterial valves, but may also be mechanically induced using an external source. SWE has been clinically successful in various non-cardiac domains, such as staging liver fibrosis (Ferraioli *et al.*, 2015) and characterizing malignant breast lesions (Barr *et al.*, 2015). The potential of the method to directly assess passive – and active – myocardial stiffness exists, but the method is faced with challenges relating to its fundamental working principles when applied to the heart. Indeed, the geometrical and mechanical properties of the heart – thin-walled, anisotropic, layered, actively contracting (in short: *mechanical factors*) – are more complex than that of large nonlinear viscoelastic organs such as the breast and the liver, evoking an altered wave physics that obeys different physical principles. With it, also the interpretation of the observed shear waves and the deduction of tissue properties becomes more complex.

This paper reviews the basic concepts of cardiac ultrasound SWE and gives an overview of the (pre)clinical studies that have investigated the effect of one or multiple mechanical factors and pathology on shear wave propagation. This way, the reader will be able to better understand shear wave measurements in the cardiac setting and interpret findings from a biophysical point of view. Shear wave speed values reported for healthy volunteers and various preclinical and patient studies (myocardial infarction, hypertrophic cardiomyopathy, amyloidosis, heart transplantation, hypertension) are summarized. The paper concludes with recommendations on uniform reporting and identification of the main mechanical (and technical) challenges ahead.

Definitions

The *stiffness* of a solid material, such as cardiac tissue, relates to the relation between its loading and subsequent deformation, typically described by the normalized physical quantities *stress* and *strain respectively*. In continuum mechanics, one typically expresses *material stiffness (*or *modulus)* as the mathematical relationship between stress and strain. In clinical practice (where it is often impossible to assess stress and strain), one often uses *structural stiffness*, which depends on material stiffness but also on its geometry and boundary conditions (Guimarães *et al.*, 2020; Fung, 1993). Biological tissue is often approximated as a *linear elastic isotropic* material in the field of elasticity imaging, in which the stress σ linearly depends on the strain ε regardless of the material's orientation (i.e. isotropy), as visualized in Figure 1a. The slope of the curve represents the *elasticity* or *Young's modulus E*, expressing the material's resistance to uniaxial tension/compression. The relative material deformation in the direction perpendicular to the loading direction is then given by *Poisson's ratio* υ. Other important moduli that describe the material's response to different kinds of loading are the *shear modulus* μ (material's resistance to simple shear loading) and the *bulk modulus* K (material's resistance to volumetric changes).

The linear elastic isotropic material model is a good first order approximation for some tissues (e.g. liver), but in general material properties of tissue are essentially dependent on material orientation (*anisotropy*), time *(viscoelasticity)* and stretch state (*material non-linearity* or *hyperelasticity)*, as shown in Figure 1. This figure also demonstrates the meaning of *instantaneous* or *operational* stiffness (local slope of the (ε,σ)-relationship): a higher instantaneous stiffness – indicated by E_{high} in Figure 1b – might be related to higher strains (hyperelastic effect), higher strain rate (viscoelastic effect) or fiber orientation (anisotropic effect). In addition, the apparent stiffness of a muscle can be modified by internal stress induced by active contraction.

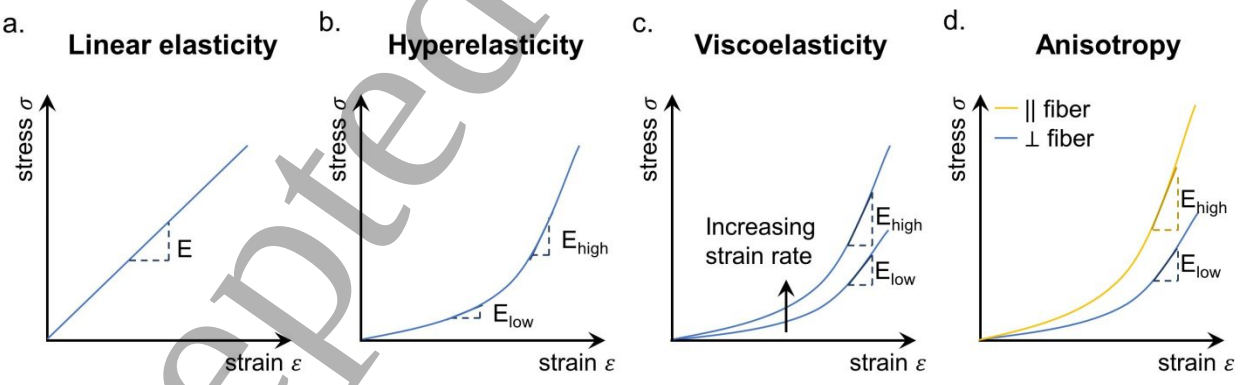

Figure 1 – Mechanical engineering definitions: conceptual representation of linear elasticity (a), hyperelasticity (b), viscoelasticity (c) and anisotropy (d) in terms of stress-strain curves.

Theoretical background – relating stiffness to wave propagation

Theoretically, only two wave modes can exist in an isotropic bulk material: a *shear* wave, and a *compressional* wave. These wave modes are distinct in the local particle motion (or deformation)

relative to the direction of propagation (see Figure 2a): a shear or transversal wave has particle motion perpendicular to the propagation direction, whereas a compressional (or longitudinal) wave particle motion parallel to the propagation direction. These compressional waves are the acoustic waves that are used for standard echography. The propagation speeds of these two wave types are linked to different tissue material properties of the medium in which they propagate. When approximating tissue as an *infinite isotropic linear elastic medium (without viscosity)*, the following relations hold true (Cobbold, 2002):

$$c_T = \sqrt{\frac{\mu}{\rho}} \tag{1}$$

$$c_L = \sqrt{\frac{K + \frac{4}{3}\mu}{\rho}} \tag{2}$$

with shear wave propagation speed c_T, shear modulus μ, mass density ρ, longitudinal wave propagation speed c_L, and bulk modulus K. A mass density of 1000 kg/m^3 is commonly assumed.

It is important to stress that pure shear and compression waves only exist in an infinite, homogenous, isotropic medium, for which Eqs. 1 and 2 describe the wave propagation velocities. These equations are only valid for plane waves, as a finite source of excitation also results in a shear wave with longitudinal polarization and a longitudinal wave with shear polarization (Catheline and Benech, 2015). This shear wave with longitudinal polarization is the base of 1D transient elastography (Catheline *et al.*, 1999; Sandrin *et al.*, 1999). Furthermore, a confined geometry or inhomogeneous and direction-dependent material properties – all of which are true for the myocardium – might evoke other wave modes than a shear wave (e.g. vertical/horizontal shear waves in transverse isotropic media (Wang *et al.*, 2013; Rouze *et al.*, 2013), Lamb waves in plate-like geometries (Caenen *et al.*, 2017; Keijzer *et al.*, 2020b)). Wave motion can then have a longitudinal component next to a transversal component. This should be considered when interpreting the mechanical waves detected with echocardiography and will be discussed in detail further in this review (see *Shear wave imaging and reconstruction of shear wave speed maps).*

In principle, both shear and bulk modulus are expected to correlate to tissue composition, and hence to disease state. However, when comparing the two wave modes in terms of clinical applicability for elasticity imaging, shear waves have been preferred for tissue characterization because: (i) their wave propagation speed has a larger range compared to longitudinal waves (speed range of 0.5-20m/s vs. 1350-1700m/s in soft tissues (Cobbold, 2002)) making it easier to distinguish differences in speed; (ii) their wave propagation speed is elevated by pathological changes (up to two orders of magnitude (Greenleaf *et al.*, 2003)) and (iii) tissue Doppler echography with a frame rate in the order of kHz can be used to track shear waves .

Shear wave speed estimation in a thin-walled viscoelastic medium such as the cardiac wall is not straightforward as a shear wave of a finite temporal length intrinsically contains a range of frequencies – as an ultrasound pulse – and these frequencies can travel at different speeds, a phenomenon which is called *speed dispersion*. In general, there are two manners to characterize

the propagation of a wave: the phase and the group speed (Rose, 2014). The phase speed is the speed with which a given frequency component of the waveform propagates, whereas the group speed is the speed with which the envelope of a pulse within a frequency band propagates as illustrated in Figure 2b (Rose, 2014). The distinction between both speed types is important, as both speed estimations are often used interchangeably in cardiac SWE for diagnosis while phase speed in general does not match with group speed in the cardiac wall for current SWE-techniques.

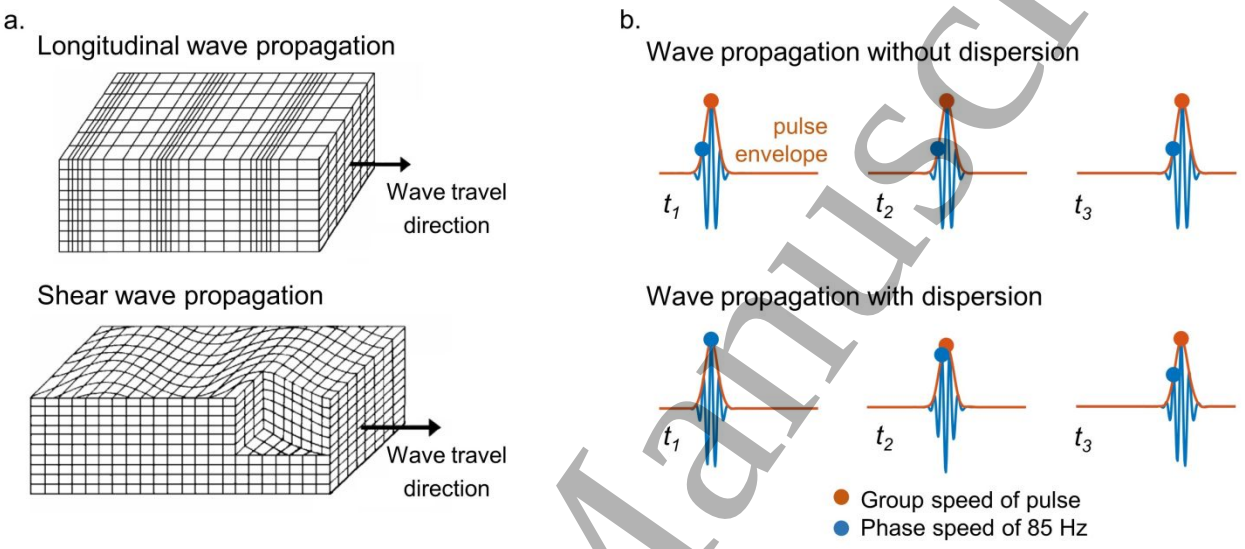

Figure 2 – Basic wave physics principles. (a) Direction of the tissue motion and wave propagation for longitudinal and shear wave propagation (adapted from (Cobbold, 2002)). (b) Concept of group and phase speed. Individual waves with a specific frequency propagate at the phase speed (blue dot); whereas the pulse envelope propagates at the group speed (orange dot).

Cardiac ultrasound shear wave elastography

Shear wave excitation sources

SWE can be realized in different manners, where the source of excitation of the shear waves is an important distinguishing criterion for cardiac SWE (see also Figure 3 and Table 1):

- Acoustic radiation force (ARF): by applying a high-intensity focused US beam for a relatively long period of time but still in an impulsive manner (< 1 ms), a localized body force is generated of a sufficiently large magnitude to evoke particle displacements in the order of a few micrometers in the direction of the US beam (Song *et al.*, 2014; Sarvazyan *et al.*, 1998; Nightingale *et al.*, 2001). In other words, the US beam literally pushes the tissue away from the transducer, while the transducer is at a distance. For cardiac SWE, the geometrical shape of the ARF is typically ellipsoidal around the US beam axis with a length encompassing the thickness of the cardiac wall (using a strongly focused US beam or a low emission frequency). The wall region of interest should be oriented parallel with the transducer surface such that the “push” excites mainly transverse motion, which is a condition best met in the parasternal long or short axis (PLAX/PSAX) view of the

interventricular septal wall for transthoracic closed-chest settings, but more non-conventional views are feasible in an open-chest setting.

- Intrinsic motion (natural waves): mechanical waves are also caused by fast transient events in the heart such as valve closure. Previous research mainly focused on the mechanical wave propagation in the left ventricle after mitral and aortic valve closure (MVC, AVC) (Vos *et al.*, 2017; Santos *et al.*, 2018; Kanai, 2005) but also after atrial kick (AK) (Pislaru *et al.*, 2014a). As the spatial and temporal properties of the excitation source are unknown, the understanding of the measured phenomena remains poor. A recent 3D study on natural waves (Papadacci *et al.*, 2020) has shown that there might be two sources of wave excitation after MVC, but these results are still very preliminary (n=3). Natural waves after valve closure contain both transversal and longitudinal components of tissue motion, explaining why analyses based on both parasternal and apical views have been reported in literature (Keijzer *et al.*, 2020b; Brekke *et al.*, 2014). Mechanical waves following AK did not reveal any wave-like pattern in the parasternal view, suggesting that AK's wave motion is predominantly longitudinal (Strachinaru *et al.*, 2019b) and therefore this wave phenomenon is not further considered in this review.
- External mechanical actuator: some studies (Urban *et al.*, 2013; Pislaru *et al.*, 2014b; Tzschatzsch *et al.*, 2012) reported the use of an actuator vibrating at a specific frequency to induce a monochromatic (i.e. single frequency) mechanical wave. This excitation method is typically used in magnetic resonance elastography (Mariappan *et al.*, 2010; Elgeti *et al.*, 2014), and has been used in ultrasound elastography as well to study the induced shear wave amplitude in healthy volunteers as a qualitative measure of stiffness (Tzschatzsch *et al.*, 2012). However, to use SWE in a more quantitative way (as reported in Table 1), the monochromatic excitation is repeated at multiple frequencies to reconstruct the frequency behavior of the shear wave for the estimation of material parameters. The use of this method has only been reported in open-chest studies (Nenadic *et al.*, 2018; Pislaru *et al.*, 2014b).

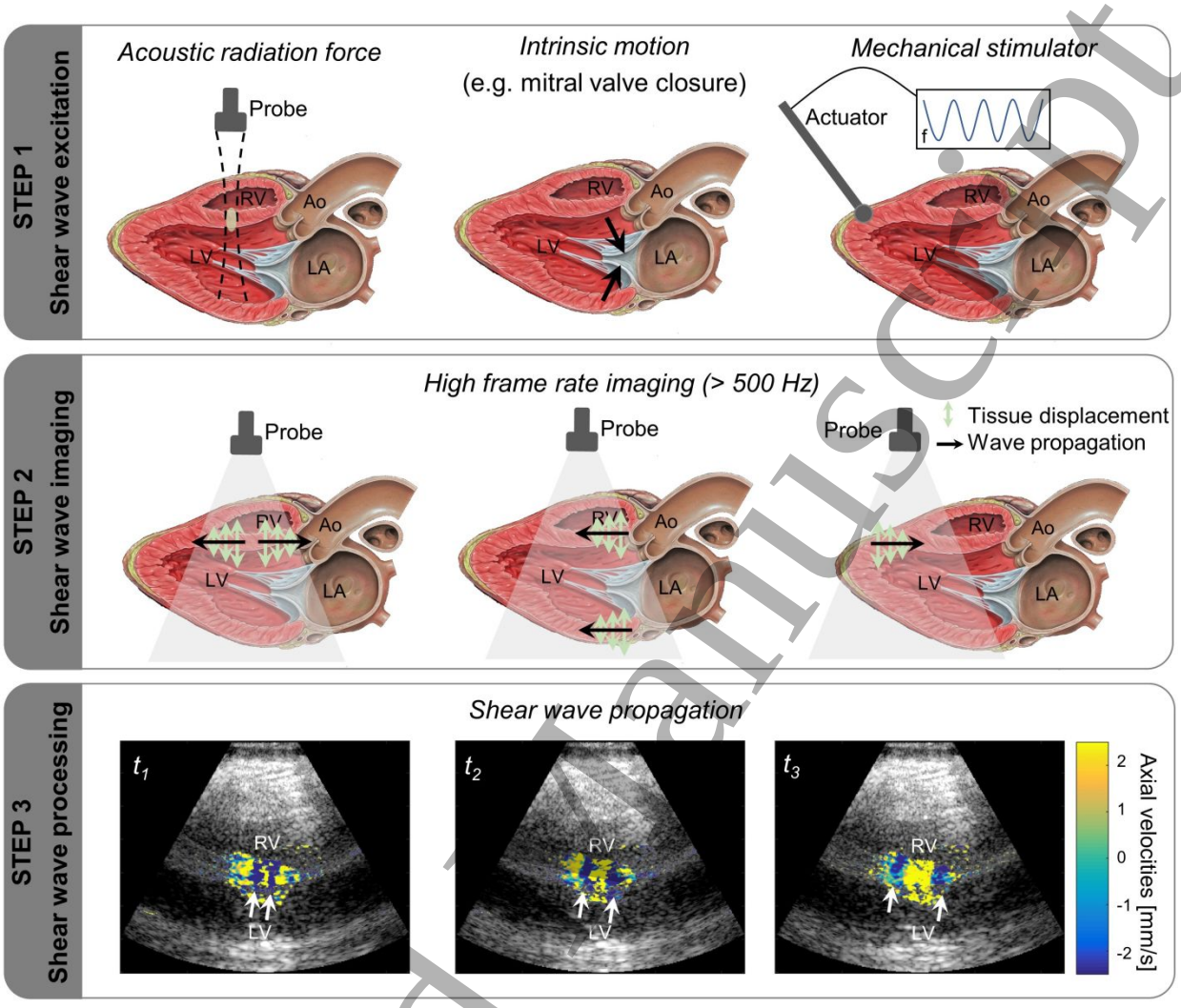

Figure 3 – Principle of ultrasound SWE in a cardiac setting (anatomical image adapted from (Olson and Pawlina, 2008)). Shear wave propagation shown as example in step 3 is measured in vivo in the interventricular septum of a closed-chest pig using an acoustic radiation force for shear wave excitation in an ongoing study (approved by the Ethical Committee for Animal Experiments of KULeuven P041/2019).

It should be noted that mechanical waves after valve closure occur at specific locations and moments in the cardiac cycle, whereas an ARF-induced shear wave is in theory fully controllable in time and space by the user, as much as the acoustic windows allow for. However, transthoracic excitation of shear waves in an acoustically safe manner remains challenging due to the limited aperture size (small acoustic windows) and small amplitude and quickly attenuating tissue motion in especially the stiff cardiac wall in systole. The use of intracardiac (Hollender *et al.*, 2012) or trans-esophageal (Kwiecinski *et al.*, 2015) transducers might offer a solution to this problem, but this comes with patient discomfort, increased health risks, and demanding technical requirements – small piezoelectric elements with enough power to generate a sufficiently large ARF. An advantage of intrinsic mechanical waves is their displacement magnitude which is one order of magnitude larger than that of ARF-induced waves (Table 1), improving the signal-to-noise ratio (SNR) of SWE. Additionally, transthoracic imaging of natural waves does not pose any problems regarding acoustic safety, permitting an easy implementation in clinical practice.

Table 1 – Overview of different wave excitation sources in ultrasonic cardiac SWE with typical application settings and shear wave properties (IVS: interventricular septum; LVW: left ventricular wall; LVFW: left ventricular free wall; NR: not reported; PLAX: parasternal long-axis view; PSAX: parasternal short-axis view).

	Excitation source	Timing	Frequency content	Tracked tissue motion	Cardiac wall location	Reported metrics
Open/closed-chest	Acoustic radiation force (impulsive)	Any instant in cardiac cycle*	<500 Hz (Sarvazyan *et al.*, 2013)	Transversal ~ 5 µm (Song *et al.*, 2014)	IVS in PLAX/PSAX LVFW (open-chest)	Group speed (Keijzer *et al.*, 2020a) Elasticity (Villemain *et al.*, 2018) Group speed (Couade *et al.*, 2011; Bouchard *et al.*, 2009) Group speed, elasticity, viscosity (Nenadic *et al.*, 2018)
	Intrinsic motion	AVC/MVC	<150 Hz (Kanai, 2005; Vos *et al.*, 2017; Pernot and Villemain, 2019)	Transversal ~ 100 µm (Vos *et al.*, 2017; Santos *et al.*, 2018) Longitudinal	Mainly IVS in PLAX IVS in AP3C/AP4C (Brekke *et al.*, 2014; Keijzer *et al.*, 2020b)	Group speed (Santos *et al.*, 2018; Salles *et al.*, 2019; Keijzer *et al.*, 2019) Group speed, phase speed (Vos *et al.*, 2017) Phase speed, elasticity, viscosity (Kanai, 2005)
Open-chest	External vibrator	Any instant in cardiac cycle	50-400 Hz in steps of 50 Hz (Pislaru *et al.*, 2014b)	Transversal 10-100 µm (Pislaru *et al.*, 2014b)	LVFW	Phase speed, elasticity, viscosity (Pislaru *et al.*, 2014b; Urban *et al.*, 2013)

* Very low success rate in systole.

Shear wave imaging and reconstruction of shear wave speed maps

High frame rate imaging (frame rate >500 Hz) is applied to visualize the propagating shear wave. The use of diverging wave imaging in a fundamental (Santos *et al.*, 2018) or pulse-inversion harmonic (Song *et al.*, 2013) manner has been reported for this purpose. Spatial resolution and contrast can be further improved by coherently compounding diverging waves emitted from multiple angles (Montaldo *et al.*, 2009) or zones (Santos *et al.*, 2018). After recording the shear wave motion, a tissue motion estimator is applied to the radio-frequency (RF) or demodulated in phase quadrature (IQ) data (e.g. a standard Doppler auto-correlator as the one described by Kasai et al. (Kasai *et al.*, 1985)). The use of tissue displacement, velocity and acceleration have been reported to visualize shear wave motion in cardiac SWE (Deng *et al.*, 2017; Nenadic *et al.*, 2018; Santos *et al.*, 2018).

For shear wave speed estimation, the first step is to select a wave propagation path along the cardiac wall which also includes the shear wave excitation source (white line in Figure 4a). The excitation source is always included in the imaging plane for ARF-induced waves as the same transducer is used to generate and detect shear waves, but attention should be paid to include the valves in the imaging plane when visualizing waves after intrinsic motion (Villemain *et al.*, 2020). A curved (anatomical) M-mode displaying tissue motion data as a function of space and time is then obtained, as illustrated in Figure 4b. Various methods have been reported in literature

to distinguish the high frequency wave motion from the low frequency gross cardiac motion in this M-mode: application of a high-pass filter on tissue motion data (Vos *et al.*, 2017; Keijzer *et al.*, 2019) (example is shown in Figure 4b-c) or on the IQ data (Salles *et al.*, 2019), subtraction of the average wall motion (Pernot *et al.*, 2016) or representation of tissue motion in the form of accelerations (Santos *et al.*, 2018). Shear wave speed estimation is then typically performed using a time-of-flight (TOF) estimator, which characterizes the shear wave's position as a function of time (see Figure 4c). The resulting speed can be classified as *phase speed* when using a single frequency source (external vibrator in Table 1), and as *group speed* when using a broadband excitation (ARF/intrinsic motion in Table 1) (Parker *et al.*, 2018). Note that the *phase speeds* of all excited frequencies in the shear wave motion can be studied by repeating the measurement at a different frequency in case of an external vibrator or performing a Fourier analysis in the frequency domain in case of ARF/intrinsic motion (*speed dispersion analysis* (Deffieux *et al.*, 2009)). Most studies report shear wave speed as an end result, whereas others convert speed c_T into Young's modulus E through equation (1) and the following equation:

$$E = 2(1+\nu)\mu \approx 3\mu \tag{3}$$

with Poisson's ratio ν (usually assumed 0.5 to describe tissue incompressibility (Fung, 1993)). Note that application of equation (3) implies that the myocardium is a priori considered an isotropic linear elastic material, and all observed wave phenomena are analyzed and interpreted within that paradigm. Unfortunately, this is an over-simplification, and it remains poorly understood how the conversion to true stiffness constants can be made accurately for the myocardium.

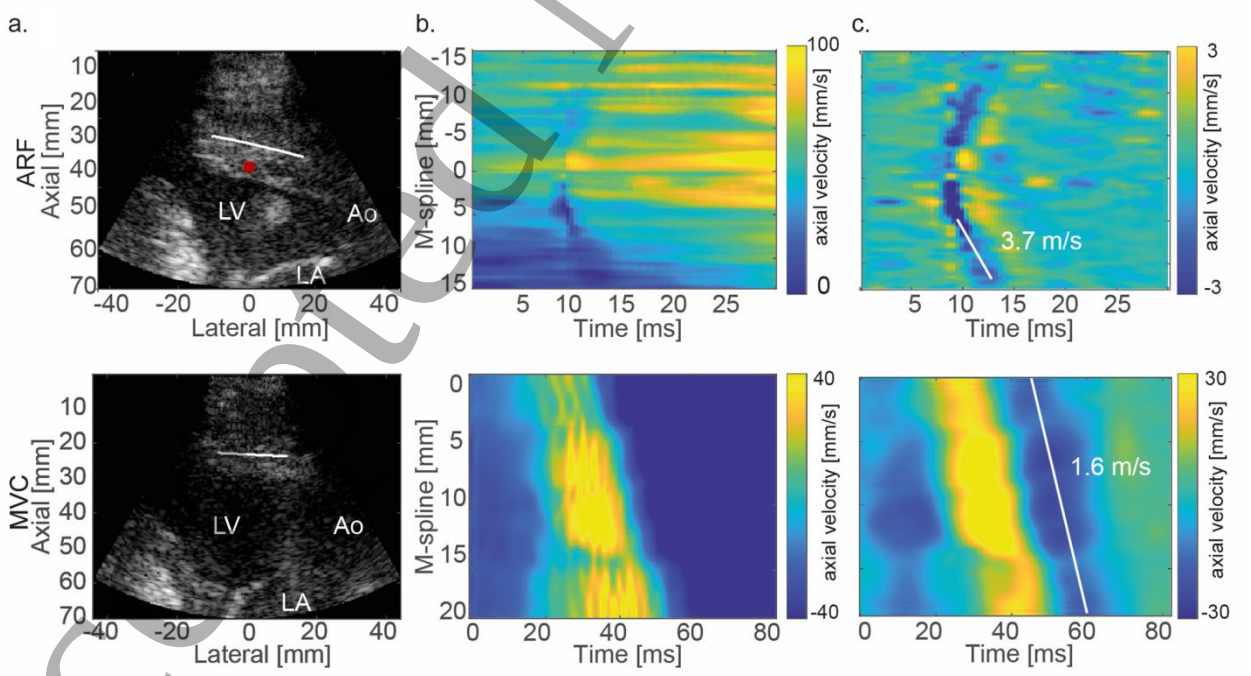

Figure 4 – Reconstruction of shear wave speed. (a) B-mode in parasternal long-axis view for acoustic radiation force (ARF) induced shear waves in the upper panel (red rectangle indicates push focus) and shear waves induced by mitral valve closure (MVC) in lower panel. (b) Measured tissue motion. (c) Measured shear wave motion after

application of band pass filter with cut-off frequencies at 75-750 Hz for ARF-induced wave and 15-100 Hz for MVC-induced wave. For ARF-based SWE, two shear waves are created in the center of the field of view (in the IVS); whereas for natural SWE one shear wave is propagating from base to apex. Adapted with permission from Keijzer and Caenen et al. (Keijzer et al., 2020a).

Recently, 3D high frame rate approaches have been reported in cardiac SWE through the use of ECG stitching (Salles *et al.*, 2020) or coupling multiple US systems (Papadacci *et al.*, 2020). Both approaches have been applied for imaging natural waves for which the wave propagation physics is less well defined than for ARF-induced waves. These 3D approaches allow to first apply a wave excitation source localization method to determine the wave propagation path for local wave speed estimation using a TOF algorithm.

Mechanical factors affecting shear wave speed in the heart – what causes complexity?

The interpretation of measured shear waves in the heart is complex due to multiple mechanical factors directly affecting shear wave speed values and interfering with effects of pathology. In this section, we review how geometry, viscosity, anisotropy, contraction/relaxation, hemodynamics, and pathology affect shear wave patterns and speed (Figure 5). We first macroscopically describe the effect of each factor on shear wave propagation and summarize its impact on reported wave speed variations in Table 2. Diastolic and systolic speeds are reported in separate columns, with the speed of the mechanical waves after MVC and AVC classified as diastolic and systolic speed, respectively (even though this classification is debatable as in some definitions the diastolic and systolic phases are ending at the moment of valve closure).

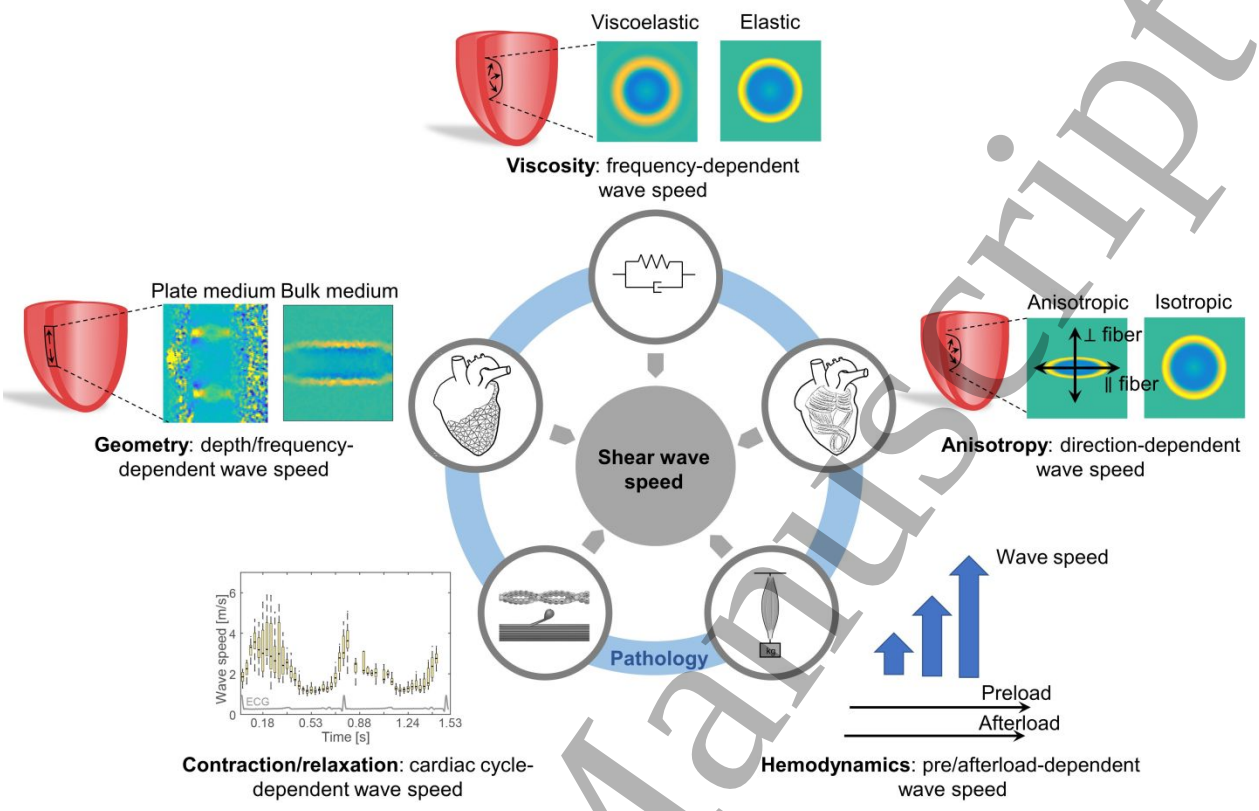

Figure 5 – Mechanical factors affecting wave speed estimation in cardiac shear wave elastography.

Geometry

Pure shear waves theoretically only exist in an infinite medium, a condition that is sufficiently met when the shear wavelength is significantly smaller than the smallest dimension of the medium in which it travels. In general, the studied wavelength in cardiac SWE depends on the selected excitation source (see Table 1), typically a few mm for ARF-induced waves and a few cm for natural waves, which is of the same order of magnitude or larger than the cardiac wall thickness (Kanai, 2005; Urban *et al.*, 2013; Nenadic *et al.*, 2018; Pislaru *et al.*, 2014b). This means that the wave will reflect from the boundaries, confining the mechanical energy within the wall (Figure 6a) leading to guided waves. The wave front might be visually distorted during propagation (Figure 6b), potentially resulting in a depth-dependent shear wave propagation speed as visualized in Figure 6b for a left ventricular phantom. Also, the wave guide can result in dispersive effects, with the phase speed increasing as a function of frequency, as illustrated in Figure 6b and tabulated in Table 2 (Rose, 2014). The nature of the shear wave is thus altered and consequently the propagation characteristics are not only dependent on stiffness – as one would conclude from equation (1) – but also on geometry, tissue surrounding and excitation characteristics. LV phantom experiments and simulations have shown that the TOF method can underestimate the true stiffness up to 35 % for ARF-based SWE depending on wall thickness and echocardiographic view (Caenen *et al.*, 2017). A recent study also investigated the effect of the thickness variations of the cardiac wall in simulations, showing a similar shear stiffness error for ARF-based SWE and an error of up to 65% for natural SWE (Sabbadini *et al.*, 2021). The Lamb wave theory on waves

in plates has been used to better understand the geometrical effect on cardiac shear wave propagation and to improve shear wave characterization methods, on which more information can be found in the appendix.

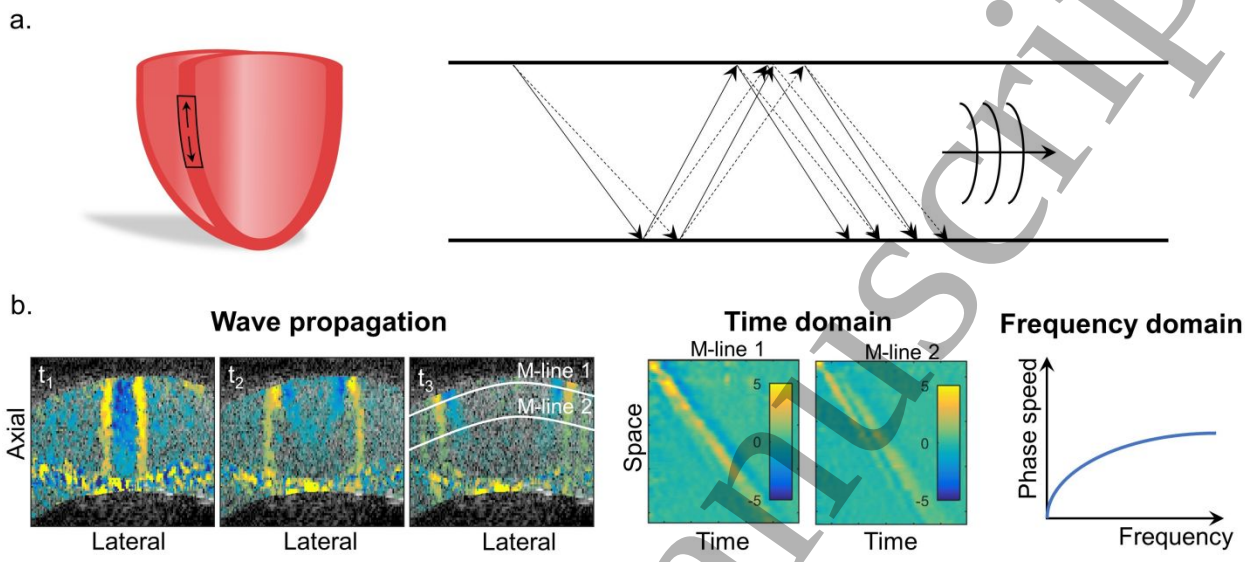

Figure 6 – Effect of geometry on shear wave properties. (a) Principle of waveguide. (b) Example of shear wave propagation in a left ventricular phantom. The two M-modes show that the shear wave propagation pattern in the time domain depends on the chosen depth. The frequency characteristics demonstrate an increasing phase speed as a function of frequency, even under the assumption of pure elasticity (no viscosity). Adapted with permission from Caenen et al. (Caenen et al., 2017).

Viscosity

Viscosity leads to absorption of the mechanical wave energy due to viscous friction, resulting in attenuation of the wave's amplitude. The viscosity-related attenuation increases with frequency, leading to a smoothed wave shape by removal of the high frequencies as shown in the Figure 5 (Bercoff *et al.*, 2004). This comes together with an apparent stiffening of the material with increasing frequency, which in turn leads to a frequency-increasing phase speed, as is conceptually illustrated in Figure 7. The range of speeds that is reported by various studies is summarized in Table 2. Often a Voigt model is assumed to describe the relationship between shear wave speed dispersion and the material parameters (Nightingale *et al.*, 2015), for which the dispersion relation is given by

$$c(\omega) = \sqrt{\frac{2(\mu^2 + \omega^2\eta^2)}{\rho(\mu + \sqrt{\mu^2 + \omega^2\eta^2})}} \qquad (4)$$

with propagation speed $c(\omega)$, angular frequency ω, shear modulus μ and shear viscosity η (see Figure 7). Some studies used this frequency-dependency to estimate myocardial viscoelasticity (Kanai, 2005; Urban *et al.*, 2013; Nenadic *et al.*, 2018; Pislaru *et al.*, 2014b), which might provide additional diagnostic value next to elasticity (Sugimoto *et al.*, 2020). For further details on this type of material characterization, we refer the reader to the appendix.

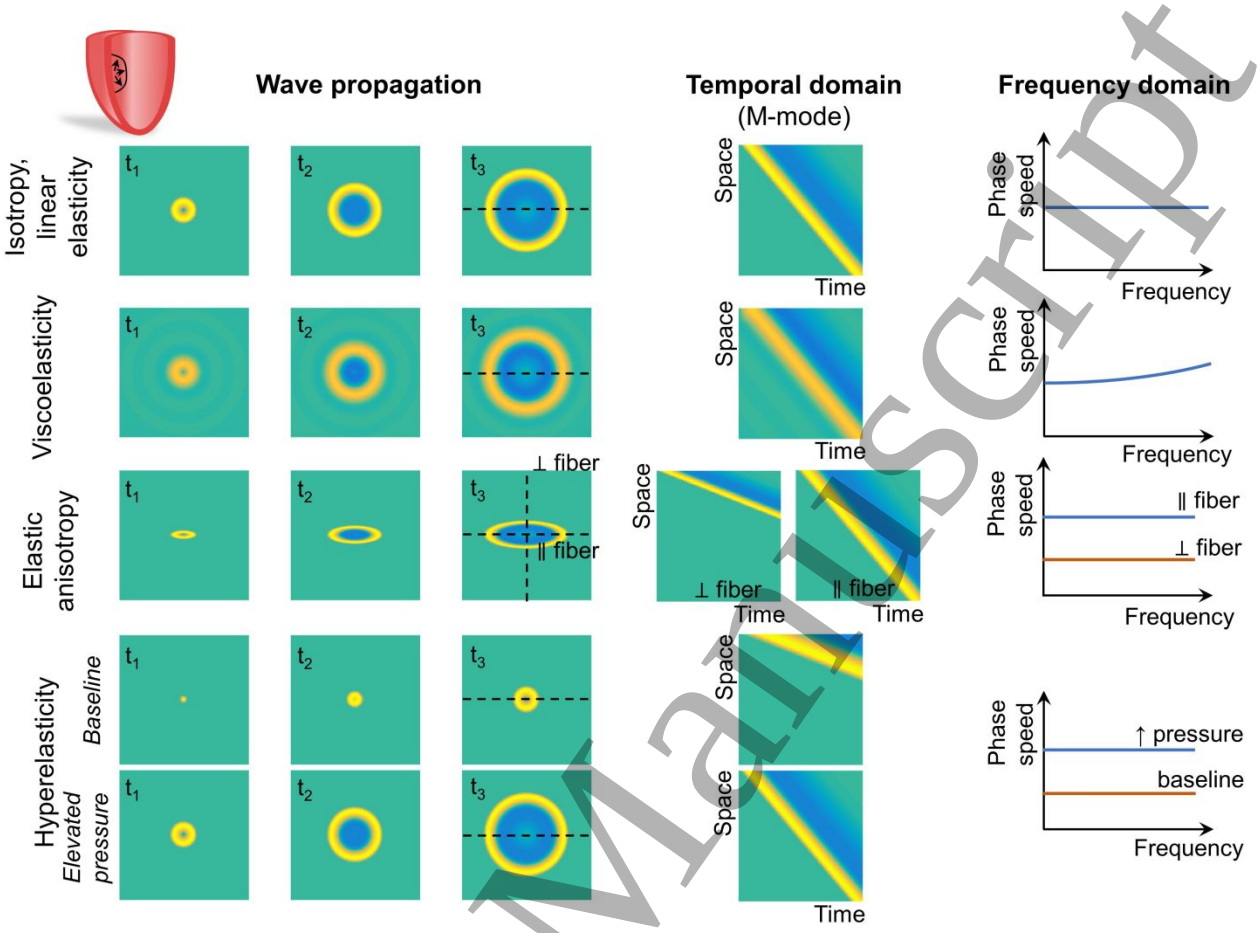

Figure 7 – Conceptual representation of the effect of viscoelasticity, elastic anisotropy and hyperelasticity on shear wave propagation, temporal and frequency characteristics.

Anisotropy

It is known from physics that shear waves propagate faster along the fiber than across due to elastic anisotropy, resulting in an elliptical shaped propagation pattern (Wang *et al.*, 2013) (see Figure 5 and Figure 7). The myocardial fiber architecture is however complex: it follows a helical arrangement and it varies transmurally. For the sake of simplicity, however, many studies have assumed that the myocardium is locally transverse isotropic, with a symmetry axis along the local direction of fiber, resulting in a transmural varying wave directionality parallel to the cardiac wall (see Figure 8a and Table 2). Note that the polarization direction of the shear wave with respect to the fiber orientation is also important. For example for an incompressible transverse isotropic medium such as skeletal muscle, two shear wave modes traveling at different speeds are possible: a shear horizontal mode, for which the wave propagation vector is perpendicular to the plane formed by the material symmetry axis and wave propagation direction, and a shear vertical mode, for which the wave propagation vector is parallel to the plane formed by the material symmetry axis and wave propagation direction (Rouze *et al.*, 2013; Knight *et al.*, 2021). These are also called slow and fast shear waves.

The anisotropy in shear wave propagation has been assessed by analyzing the transmural wave speed variations in 3D (see Figure 8b) or in two echocardiographic views (Figure 8c). For example, wave speed in PSAX is higher than in PLAX at the mid cardiac wall for both ARF-induced (Villemain *et al.*, 2018) and natural waves (Papadacci *et al.*, 2020). Some studies have used this anisotropy in wave propagation to extract the myocardial fiber orientation, which agreed well with histology (Lee *et al.*, 2012b) and magnetic resonance diffusion tensor imaging (Lee *et al.*, 2012a). Other studies suggest that anisotropy of wave propagation offers additional diagnostic value (Villemain *et al.*, 2018). In that respect, Couade et al. (Couade *et al.*, 2011) introduced a new parameter, called *fractional anisotropy* (FA), to estimate the degree of anisotropy:

$$FA = \frac{\sqrt{(v_{PSAX} - \overline{v})^2 + (v_{PLAX} - \overline{v})^2}}{\sqrt{v_{PSAX}^2 - v_{PLAX}^2}} \quad (5)$$

With v_{PSAX} the speed in PSAX, v_{PLAX} the speed in PLAX and $\overline{v}$ the average of v_{PSAX} and v_{PLAX}. FA can be calculated at any transmural depth, as shown in Figure 8c for the LV free wall in an open-chest sheep in diastole and systole (Couade *et al.*, 2011). Villemain et al. (Villemain *et al.*, 2018) reported a FA of 0.238±0.068 for the mid cardiac wall in healthy volunteers, and a decreased FA of 0.133±0.073 in patients with hypertrophic cardiomyopathy (HCM).

a. **Anisotropic shear wave propagation in cardiac SWE simulations:**
shear wave pattern and 3D shear wave propagation speed map

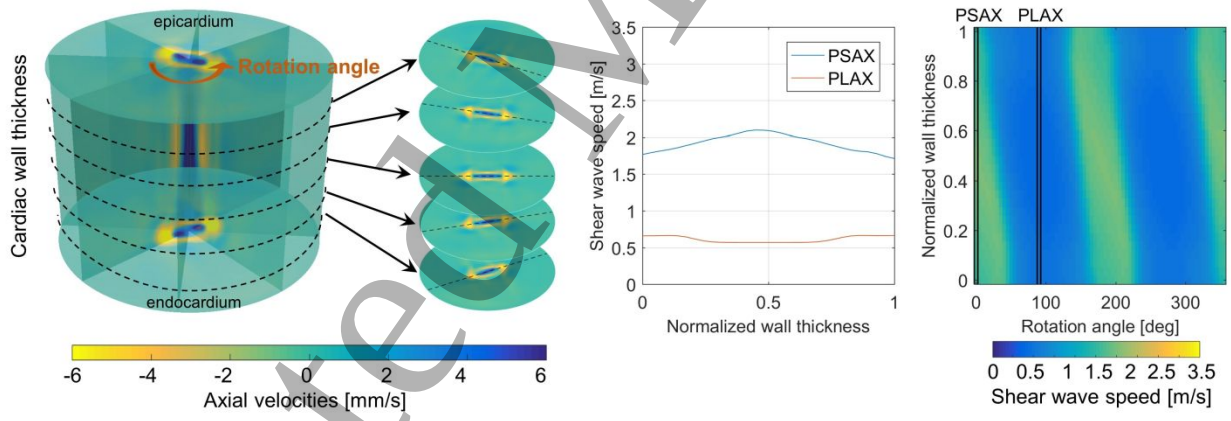

b. **Shear wave propagation in in vivo open-chest sheep:**
Diastolic and systolic shear wave propagation speed in PLAX and PSAX

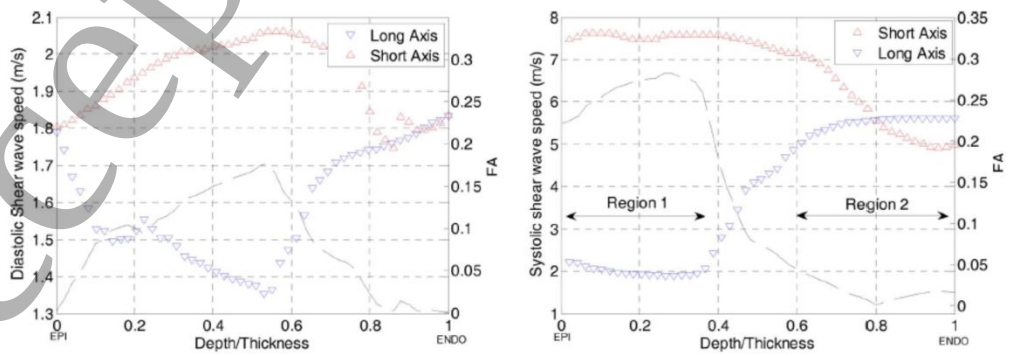

Figure 8 – Effect of anisotropy on shear wave properties for ARF-induced shear waves. (a) Demonstration of the ellipsoidal wave propagation patterns for various slices across cardiac wall thickness in a computer model of cardiac SWE (Caenen et al., 2018). The black dotted line in the slices represents the actual myocardial fiber orientation in the model. A shear wave propagation speed map can be obtained when analyzing the wave propagation for every angle in each transmural slice. The maximal speed in this map corresponds approximately to the myocardial fiber orientation (Caenen et al., 2018). Adapted with permission from Caenen et al. (Caenen et al., 2018). (b) Transmural shear wave speed and fractional anisotropy variations in diastole and systole of the LVFW of an open-chest sheep. Adapted with permission from Couade et al. (Couade et al., 2011).

Contraction/relaxation

Besides passive material properties, cardiac contraction affects shear wave speed measurements (see Table 2), providing opportunities for assessing time-varying muscle stiffness and, hence, myocardial contractility. Indeed, Bézy et al. (Bezy *et al.*, 2020a) found a positive linear correlation between the wave speed after AVC and end-systolic elastance ($R=0.640$; $p<0.001$) after dobutamine administration and bicycle exercise. Application of ARF-based SWE in a Langendorff animal heart set-up allowed to relate the shear wave speed in systole to the inotropic state of the heart in an unloaded condition: systolic shear stiffness was linearly correlated to coronary perfusion pressure (slope of 0.27 kPa/mmHg or, recalculating to shear wave speed[1], 0.52 m/s/mmHg; $R^2=0.73$ (Vejdani-Jahromi *et al.*, 2017)) and to systolic pressure during administration of isoproterenol ($R^2=0.94$-0.98; $p<0.0001$ (Pernot *et al.*, 2011)). Furthermore, repeated application of ARF-based SWE throughout the cardiac cycle allows to capture the dynamic stiffness variations (see Figure 9c). Two studies of the same authors (Vejdani-Jahromi *et al.*, 2018; Vejdani-Jahromi *et al.*, 2016) have used the wave speed variations during the isovolumic relaxation phase to estimate the relaxation time constant of diastolic function. The researchers reported an average time constant of 65±19 ms for 8 Langendorff perfused rabbit hearts, which increased to 154±60 ms after MI induction. Furthermore, a linear regression model demonstrated the similarity between the relaxation time constant obtained from the LV pressure curve and the ARF-based shear wave speed curve (slope=1.164; $R^2=0.8$ (Vejdani-Jahromi *et al.*, 2018)).

It should, nonetheless, be noted that the timing of the mechanical waves after valve closure within the isovolumic contraction/relaxation phase is unclear. Recent work combining ARF-based and natural SWE (Keijzer *et al.*, 2020a) was able to detect both wave types in the same acquisition as visualized in Figure 9a and b. This permitted to investigate the timing of natural wave measurements with respect to ARF-assessed cardiac dynamics: waves after valve closure occurred when the myocardium is in between relaxation and contraction (Figure 9c). Additionally, this figure shows a good match in propagation speeds between natural and ARF-based SWE at the moment of valve closure, despite the clear differences in wavelength (a few mm vs. a few cm) and wave amplitude (a few mm/s vs. tens mm/s) (Figure 9a-b). This result shows that many factors, such as fluid loading, contraction speed, contraction synchronicity, or even stenosis of outflow track or mitral valve, can affect the exact moment of valve closure, and hence the instantaneous speed of the induced wave.

[1] Recalculated from equation (1) while assuming a density of 1000 kg/m^3.

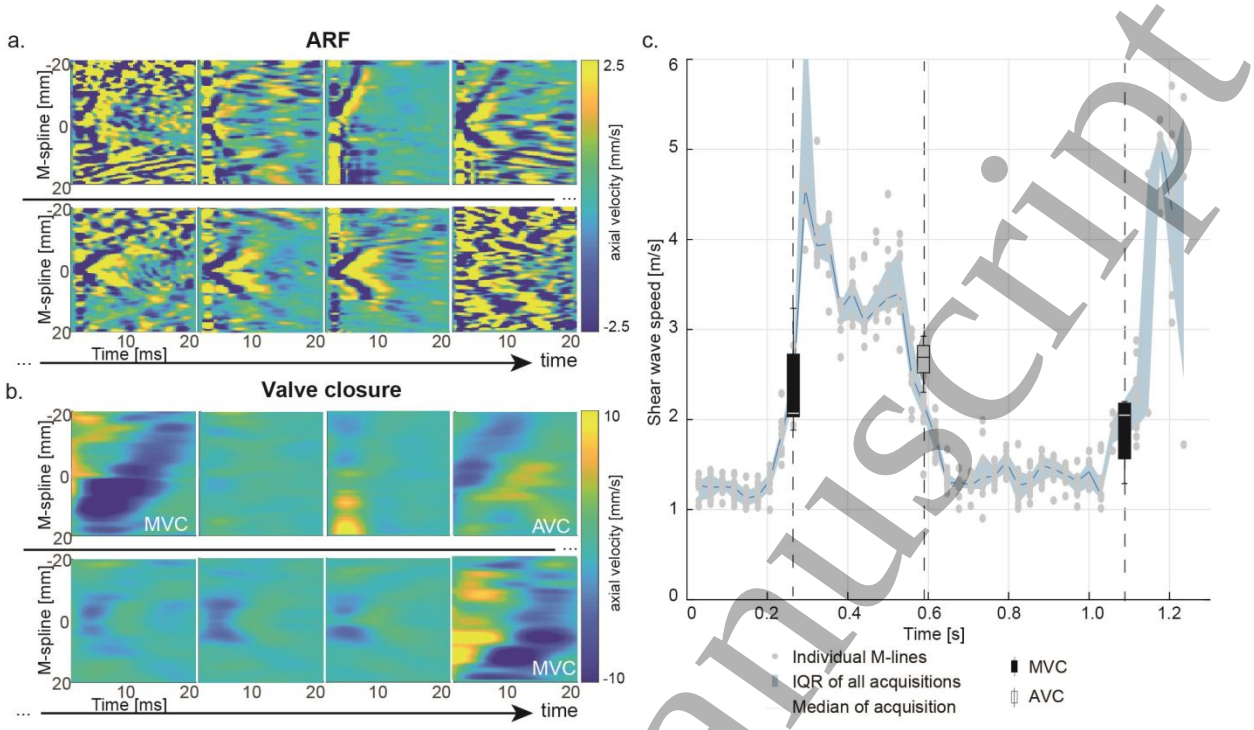

Figure 9 – Shear wave propagation throughout the cardiac cycle in a pig's septal wall. Two types of shear waves are visible in the same SWE acquisition: shear waves induced with an acoustic radiation force (ARF; panel a) and by valve closure (VC; panel b). Panel c demonstrated the estimated shear wave speeds for both techniques. Adapted with permission from Keijzer and Caenen et al. (Keijzer et al., 2020a).

Hemodynamics

Altering preload or afterload affects the magnitude of the pressure acting on the cardiac wall, and thus the stress/strain state in the ventricle because of the material's hyperelasticity (see Figure 1b and Figure 7). Table 2 quantifies the effect of changing loading condition on the wave speeds. A negligible change in diastolic wave speed was reported for ARF-based SWE (Δ0.04 m/s for ΔEDP of 14.7 mmHg (Pernot *et al.*, 2011) and Δ0.5 kPa for ΔEDP of 5 mmHg (Pislaru *et al.*, 2014b)), whereas the wave speed after MVC increased significantly with increased EDP (Δ4.9 m/s for ΔEDP of 21.7 mmHg: R=0.83 and p<0.001 (Bezy *et al.*, 2020b)). Differences in shear wave excitation properties, experimental set-up and investigated pressure range partly explain the reported difference in the sensitivity of shear wave speed to pressure, but more importantly, the end-diastolic moment of the shear wave recording for ARF-based SWE might still be in the quasi-linear part of the stress-strain relationship whereas this might be different for the shear wave after MVC for which, again, the exact timing within the isovolumic contraction phase is unclear (Keijzer *et al.*, 2020a; Pernot and Villemain, 2019).

Pathology

Most literature on SWE in pathology is obtained in animal models (Pernot *et al.*, 2016; Couade *et al.*, 2011; Pislaru *et al.*, 2014b) by inducing a myocardial infarction (MI) through ligation of a coronary artery using ARF-based SWE. Studies have consequently reported an increase in diastolic wave speed following MI (range of Δ0.11-2.18 m/s for all studies; Table 2), of which its

magnitude depended on the duration of ligation (15-120 minutes) and reperfusion (40-120 minutes). A short term ligation of 15 minutes did not affect diastolic wave speed permanently (Couade *et al.*, 2011; Pernot *et al.*, 2016). The increase in diastolic wave speed after MI was validated, by comparison with several invasive measurements: (i) an increase in the exponential coefficient of the end-diastolic pressure volume relationship (4.027 vs. 2.010 ml^{-1}) (Vejdani-Jahromi *et al.*, 2018), (ii) an increase in the exponential coefficient of the end diastolic strain-stress relationship measured with sonomicrometry (25.7±9.5 vs. 8.8±2.3) (Pernot *et al.*, 2016) and (iii) an increase in the shear modulus obtained with the pressure-segment length method (9.4±4.9 kPa vs. 1.9±0.5 kPa) (Pislaru *et al.*, 2014b). Fewer studies (Hollender *et al.*, 2013; Couade *et al.*, 2011; Pislaru *et al.*, 2014b) also investigated the effect of MI on systolic wave speed, but the results are inconclusive.

Cardiac pathology might be associated with other changes next to an increased wall stiffness such as an increased wall thickness (hypertrophy), a change in viscosity and fiber disarray – especially when tissue remodeling and fibrosis occurs. Conceptually, more parameters than shear wave speed are necessary to completely describe the effect of pathology, but the clinical relevance of additional parameters needs further investigation. For example, Pislaru et al. (Pislaru *et al.*, 2014b) showed an increase in elasticity and viscoelasticity at end-diastole after reperfusion, whereas less consistent changes were found during systole.

Table 2 – Overview of (pre)clinical feasibility studies that have investigated the effect of one or more mechanical factors on wave propagation speed (ARF: acoustic radiation force; EDP: end-diastolic pressure; ESP: end-systolic pressure; FFT: fast Fourier transform; ICE: intracardiac echocardiography; LAD: left anterior descending coronary artery; LCX: left circumflex coronary artery; MI: myocardial infarct; MS: mechanical stimulation; VC: valve closure; LVFW: left ventricular free wall; other abbreviations are as listed in Table 1).

	Study description (ref #)	**Study set-up/results**				
		Excitation	**Region**	**Species**	**Diastolic wave speed [m/s]**	**Systolic wave speed [m/s]**
Geometry & viscoelasticity	Analyze frequency content using FFT (Nenadic *et al.*, 2018)	ARF	LVFW	Open-chest pig (n=1)	NR	2.2 m/s at 100 Hz to 4.8 m/s at 500 Hz
	Determine phase speed at various frequencies (Urban *et al.*, 2013)	MS	LVFW	Open-chest pigs (n=8)	1.1±0.2 m/s at 50 Hz 1.5±0.3 m/s at 100 Hz 1.6±0.4 m/s at 150 Hz 1.7±0.2 m/s at 200 Hz 2.1±0.5 m/s at 250 Hz 2.4±0.4 m/s at 300 Hz 2.5±0.5 m/s at 350 Hz	3.2±0.9 m/s at 50 Hz 3.0±0.6 m/s at 100 Hz 3.3±0.5 m/s at 150 Hz 3.8±0.6 m/s at 200 Hz 4.2±0.6 m/s at 250 Hz 4.5±0.9 m/s at 300 Hz 5.0±1.2 m/s at 350 Hz
	Determine phase speed at various frequencies (Pislaru *et al.*, 2014b)	MS	LVFW	Open-chest pigs (n=10)	1.4±0.4 m/s at 100 Hz 1.5±0.5 m/s at 150 Hz 1.6±0.2 m/s at 200 Hz 2.1±0.5 m/s at 250 Hz 2.4±0.3 m/s at 300 Hz 2.5±0.5 m/s at 350 Hz	3.1±0.5 m/s at 100 Hz 3.8±1.6 m/s at 150 Hz 4.4±2.0 m/s at 200 Hz 4.1±0.6 m/s at 250 Hz 4.4±1.0 m/s at 300 Hz 4.8±1.3 m/s at 350 Hz
	Analyze frequency content using FFT (Kanai, 2005)	VC	IVS	Human (n=5)	NR	1-2 m/s at 20 Hz 3-4 m/s at 50 Hz 3-7 m/s at 90 Hz
	Analyze frequency content using FFT (Vos *et al.*, 2017)	VC	IVS	Pig (n=22)	2.0 m/s at 15-45 Hz 2.6 m/s at 45-75 Hz 3.8 m/s at 75-110 Hz 3.4 m/s at 110-150 Hz	3.8 m/s at 15-45 Hz 3.8 m/s at 45-75 Hz 4.4 m/s at 75-110 Hz 4.1 m/s at 110-150 Hz

Anisotropy	Analyze different depths and views (Couade *et al.*, 2011)	ARF	LVFW	Open-chest sheep (n=10)	Mid: 1.5±0.3 m/s in PLAX; 1.9±0.2 m/s in PSAX Epi: 1.8 m/s in PLAX and PSAX Endo: 1.8 m/s in PSAX and PSAX	Mid: 4.8±1.4 m/s in PLAX; 6.2±1.9 m/s in PSAX Epi: 2.2 m/s in PLAX; 7.4 m/s in PSAX Endo: 5.7 m/s in PLAX; 5.0 m/s in PSAX
	Analyze PSAX and PLAX (Villemain *et al.*, 2018)	ARF	IVS	Human (n=60)	1.54±0.26 m/s in PLAX 2.16±0.42 m/s in PSAX	NR
	Analyze different axial and lateral locations (Bouchard *et al.*, 2009)	ARF	LVFW	Open-chest dog (n=1)	0.82-2.65 m/s depending on location	NR
	Analyze different axial and lateral locations (Keijzer *et al.*, 2018)	VC	IVS	Open-chest pigs (n=3)	NR	5.7-10.1 m/s depending on location
	Analyze wave propagation in 3D (Papadacci *et al.*, 2020)	VC	IVS	Human (n=3)	2.8±0.5 m/s in PLAX 4.6±0.7 m/s in PSAX	3.4±0.1 m/s in PLAX 3.5±0.3 m/s in PSAX antero-septal 5.4±0.7 m/s in PSAX postero-septal
Contraction/relaxation	Administer isoproterenol (10^{-8} mol/l) (Pernot *et al.*, 2011)	ARF	LVFW	Langendorff rat (n=6)	NR	*Pre: 3.18 m/s* *Post: 4.84 m/s*
	Changing Krebs extracellular calcium concentration (Pernot *et al.*, 2011)	ARF	LVFW	Langendorff rat (n=6)	*0.8 mMol: 1.00 m/s* *1.8 mMol: 1.01 m/s* *2.5 mMol: 1.01 m/s*	*0.8 mMol: 1.66 m/s* *1.8 mMol: 2.95 m/s* *2.5 mMol: 3.61 m/s*
	Alter coronary perfusion pressure (0-90 mmHg) (Vejdani-Jahromi *et al.*, 2015)	ARF	LVFW	Langendorff rabbit (n=8)	1.36±0.08 m/s at 0 mmHg 1.58±0.05 m/s at 25 mmHg 1.84±0.05 m/s at 50 mmHg 2.03±0.05 m/s at 75 mmHg 2.34±0.15 m/s at 90 mmHg	NR
	Alter coronary perfusion pressure (0-90 mmHg) (Vejdani-Jahromi *et al.*, 2017)	ARF	LVFW	Langendorff rabbit (n=12)	NR	*3.16 m/s at 0 mmHg* *4.09 m/s at 25 mmHg* *4.85 m/s at 50 mmHg* *5.50 m/s at 75 mmHg* *5.86 m/s at 90 mmHg*
	Perform dobutamine stress test (Santos *et al.*, 2018)	VC	IVS	Human (n=1)	Pre: 2.9 m/s 10 µg/(kg·min): 15.5 m/s 40 µg/(kg·min): 19.7 m/s	NR
	Perform supine bicycle exercise test (66 % work load) (Bezy *et al.*, 2020a)	VC	IVS	Human (n=11)	NR	Pre: 3.3±0.5 m/s Post: 6.2±1.7 m/s
	Perform dobutamine stress test (Bezy *et al.*, 2020a)	VC	IVS	Human (n=9)	NR	Pre: 4.4±0.6 m/s 40 µg/(kg·min): 7.2±1.7 m/s
Hemodynamics	Increase preload (EDP: 5.8±0.7 to 20.5±6.9 mmHg; ESP: 72±7.4 to 124.7±13.5 mmHg) (Pernot *et al.*, 2011)	ARF	LVFW	Langendorff rat (n=6)	*Pre: 1.30 m/s* *Post: 1.34 m/s* (Δ +0.04 m/s)	*Pre: 3.18 m/s* *Post: 3.51 m/s* (Δ +0.33 m/s)
	Reduce preload (ΔEDP= -10.1±2.5 mmHg) (Bezy *et al.*, 2020b)	VC	IVS	Pigs (n=5)	Δ -1.2±1.4 m/s	NR

	Increase preload (ΔEDP= +2.3±2.7 mmHg) (Bezy *et al.*, 2020b)	VC	IVS	Pigs (n=5)	Δ +2.0±0.8 m/s	NR
	Increase afterload (ΔEDP=+2.3±2.1 mmHg) (Bezy *et al.*, 2020b)	VC	IVS	Pigs (n=5)	Δ +1.9±0.7 m/s	NR
Pathology	Induce MI by 1-3h ligation of mid to distal LAD and 1-2h reperfusion (Pislaru *et al.*, 2014b)	MS	LVFW	Open-chest pigs (n=10)	2.7±1.0 m/s at 100 Hz 2.9±0.7 m/s at 150 Hz 3.3±1.3 m/s at 200 Hz 3.5±1.1 m/s at 250 Hz 3.4±0.6 m/s at 300 Hz 3.4±0.8 m/s at 350 Hz	5.4±2.4 m/s at 100 Hz 4.6±1.4 m/s at 150 Hz 4.8±0.8 m/s at 200 Hz 5.6±0.6 m/s at 250 Hz 5.0±0.6 m/s at 300 Hz 5.6±1.0 m/s at 350 Hz
	Induce MI by 2h ligation of LAD diagonal branch and 2h reperfusion (Pernot *et al.*, 2016)	ARF	LVFW	Open-chest sheep (n=10)	*Pre: 1.30 m/s* *Post MI: 2.49 m/s* *Post reperfusion: 3.48 m/s*	NR
	Induce MI by 15 min ligation of LAD diagonal branch and 40 min reperfusion (Pernot *et al.*, 2016)	ARF	LVFW	Open-chest sheep (n=10)	*Pre: 1.34 m/s* *Post MI: 1.45 m/s* *Post reperfusion:1.52 m/s*	NR
	Induce MI by 20 min ligation of LAD (Couade *et al.*, 2011)	ARF	LVFW	Open-chest sheep (n=1)	Pre: 1.5±0.1 m/s Post MI: 1.3±0.1 m/s	Pre: 6.0±0.2 m/s Post MI: 1.3±0.1 m/s
	Induce global MI by stopping inflow perfusion for 10 min and re-perfuse heart for 10 min (Vejdani-Jahromi *et al.*, 2018)	ARF	LVFW	Langendorff rabbit (n=11)	*Pre: 2.31 m/s* *Post MI: 3.29 m/s*	NR
	Induce MI by ligating LAD and LCX for 130±24 days (Hollender *et al.*, 2013)	ARF (ICE)	IVS	Pigs (n=4)	Pre: 1.41±0.10 m/s Post MI: 1.44±0.06 m/s	NR

Derived from graph or calculated from text

Converted from stiffness to shear wave speed by using equation (1) and assuming a ρ of 1000 kg/m^3

Clinical application

Shear wave speeds in healthy volunteers and patients

Various clinical studies have confirmed that mechanical factors do affect shear wave speed, and should be considered when interpreting SWE data. An overview is given in Table 3. Indeed, shear wave speed has been shown to significantly and positively correlate with ED wall thickness and with loading conditions (reflected by predictors E/e', pulmonary capillary wedge pressure, left atrial volume index or LA diameter). Additionally, a positive correlation was found between shear wave speed and age (Villemain *et al.*, 2018; Cvijic *et al.*, 2020; Bezy *et al.*, 2020c).

Table 3 – Summary of reported significant correlations between shear wave speed and parameters quantifying cardiac function in various clinical studies using univariate and multivariate analyses (ED: end diastolic; EDP: end diastolic pressure; HCM: hypertrophic cardiomyopathy; HT: hypertension; HTX: heart transplantation; HV: healthy volunteer ; LA ø: left atrial diameter; LAVI: left atrial volume index; LGE: late gadolinium enhancement; LV: left ventricle; NS: not significant; PCWP: pulmonary capillary wedge pressure; other abbreviations are as listed in Tables 1 and 2).

	Study (ref #)	Excitation	Patient	Age	Geometry	Hemodynamics		Pathology
					ED wall thickness	LA size	LV EDP	
Univariate	(Villemain *et al.*, 2018)	ARF	HV & HCM	R=0.881	NS	LAVI: R=0.623	E/e': R=0.783	LGE: R=0.804 T1 pre-contrast: R=0.711
	(Strachinaru *et al.*, 2019a)	VC	HV & HCM	NS	NR	NR	E/e': AVC: R=0.587* MVC: R=0.817*	NR
	(Petrescu *et al.*, 2019)	MVC	HV & amyloidosis	NR	NR	NR	E/e': R=0.74	NR
	(Petrescu *et al.*, 2020)	MVC	HTX	NR	NR	NR	PCWP: R=0.54	Native T1: R=0.75
	(Cvijic *et al.*, 2020)	MVC	HV & arterial HT	NR	R=0.786	LA ø: R=0.800	E/e': R=0.567	NR
	(Bezy *et al.*, 2020c)	MVC	HV & different cardiomyopathies	R=0.31	R=0.65	LAVI: R=0.38	E/e': R=0.50	Study group: R=0.54
Multivariate	(Cvijic *et al.*, 2020): R=0.857*	MVC	HV & arterial HT	β=0.015	NR	LA ø: β=1.353	NR	Study group: β=0.932
	(Bezy *et al.*, 2020c): R=0.74*	MVC	HV & different cardiomyopathies	NR	β=0.36	LAVI: β=0.20	E/e': β=0.19	Study group: β=0.24

*Converted R^2 to R.

A summary of the reported wave speeds in literature together with aforementioned study parameters can be found in Table 4. Other relevant factors for shear wave speed interpretation are the used echocardiographic view and system (Palmeri *et al.*, 2021). The manner of describing tissue motion (velocity/acceleration) is also mentioned in this table, as this affects the wave's frequency content and consequently the wave speed through dispersive effects (Trutna *et al.*, 2020). Table 4 shows higher speeds for waves after MVC and AVC than for ARF-induced waves at end-diastole. However, it is difficult to interpret the absolute speed values of both techniques since their timing and wave nature might be different (see Figure 9). Wave speeds in patients were in general higher than those in healthy volunteers.

Table 4 – Overview of reported shear wave speed values in healthy volunteer and patient studies with n≥10. For SWE based on intrinsic motion, speeds at MVC are tabulated as diastolic speeds and speeds at AVC are denoted as systolic speeds (abbreviations are as listed in Table 1, 2 and 3). In the column 'motion', 'a' means tissue acceleration and 'v' means tissue (Doppler) velocity are used for wave speed estimation.

		Study (ref #)	Population						System	Motion	Region	View	Wave speeds	
			n	Age [yrs]	ED wall thickness [mm]	LAVI [ml/m²]	LA ø [mm]	E/e' [-]					Diastole [m/s]	Systole [m/s]
Healthy volunteers	VC	(Brekke *et al.*, 2014)	10	NR	NR	NR	NR	NR	GE Vingmed	a	IVS	AP4C	NR	5.41±1.28
		(Keijzer *et al.*, 2020b)	10	29.8±6.2	NR	NR	NR	NR	Zonare	v	IVS	PLAX/ AP4C	NR	PLAX: 3.7±0.4 AP4C: 5.7±1.8
		(Keijzer *et al.*, 2019)	10	29.8±6.2	NR	NR	NR	NR	Zonare/ Philips iE33	v	IVS	PLAX	Zonare: 3.4±1.0	Zonare: 3.8±0.4 Philips iE33: 3.2±0.9
		(Petrescu *et al.*, 2019)	50	37.3	10.0	26.0	NR	6.3	HD-pulse	a	IVS	PLAX	3.54±0.93	3.75±0.76
		(Santos *et al.*, 2018)	30	30.9±5.1	9.1±1.4	NR	NR	NR	HD-pulse	a	IVS	PLAX	3.2 ± 0.6	3.5 ± 0.6
		(Strachinaru *et al.*, 2019a)	20	45±13	9±1	NR		8±1	Phillips iE33	v	IVS	PLAX	4.65±0.77	3.61±0.46
		(Cvijic *et al.*, 2020)	26	55±15	10±1	31±6	33±4	6.8±1.5	HD-pulse	a	IVS	PLAX	4.04±0.96	NR
	ARF	(Song *et al.*, 2016)	10	34	11.3±1.26	NR	NR	NR	Verasonics	v	IVS	PLAX/ PSAX	PLAX: 1.45±0.14 PSAX: 1.81±0.19	NR
											LV anterior	PLAX/ PSAX	PLAX: 1.77±0.28 PSAX: 1.96±0.38	NR
		(Villemain *et al.*, 2018)	60	50.6±16.9	5.9±1.4	25.9±8.7	NR	5.9±2.4	Aixplorer	v	IVS	PLAX/ PSAX	PLAX: 1.54±0.26 PSAX: 2.16±0.42	NR
Patients	VC	Amyloidosis (Petrescu *et al.*, 2019)	18	68.0	16.0	37.6	NR	18.0	HD-pulse	a	IVS	PLAX	6.33±1.63	5.63±1.13
		HCM (Strachinaru *et al.*, 2019a)	20	48±13	17±5	NR	NR	17±9	Phillips iE33	v	IVS	PLAX	6.88±1.22	5.13±0.68
		Arterial HT with hypertropic LV remodeling (Cvijic *et al.*, 2020)	33	59±14	14±2	38±10	40±7	8.8±2.7	HD-pulse	a	IVS	PLAX	5.83±1.20	NR
		Heart transplantation (Petrescu *et al.*, 2020):	42	54±17.8	13.3±3.1	50.2	NR	8.3±3.1	HD-pulse	a	IVS	PLAX	5.00±2.04	NR
	ARF	HCM: (Villemain *et al.*, 2018)	20	57±17.5	20.8±5.1	43.4±18.9	NR	16.1±6.5	Aixplorer	v	IVS	PSAX	3.56±1.71*	NR

*Converted from stiffness to shear wave speed by using equation (1) and assuming *a ρ of 1000 kg/m³*

Feasibility, reproducibility and availability

For ARF-based SWE, Song et al. (Song *et al.*, 2016) reported good success rates (>66.7 %) for four out of seven studied echocardiographic views at end-diastole (n=10): LV posterior free wall in PSAX; basal IVS in PSAX; mid-IVS in PSAX and basal IVS in PLAX. Furthermore, the first two views showed the highest repeatability across three different days. Villemain et al. (Villemain *et al.*, 2018) reported a 100 % success rate when studying ARF-induced shear waves in the IVS in PLAX and PSAX (n=80) – after excluding subjects based on predefined criteria (echogenicity and presence of scar due to earlier infarct). Additionally, the authors in (Villemain *et al.*, 2018) found no statistical difference between measurements at baseline and after three months (n=15). Even though the feasibility of ARF-based SWE throughout the cardiac cycle is not yet studied in the clinics, a previous preclinical study (Keijzer *et al.*, 2020a) reported a success rate of 32 % for 65 ARF-based SWE acquisitions (n=4). This demonstrates the SNR challenges for in vivo ARF-based SWE.

The reproducibility of natural SWE measurements in the heart has been more extensively studied. Studies report in general a high success rate (e.g. 94 % for AVC and 84 % for MVC for n= 63 (Petrescu *et al.*, 2019)), when excluding subjects with cardiac arrhythmias, histological or clinical evidence of allograft rejection, significant LCA stenosis, more than moderate valvular disease and poor echogenicity. Healthy volunteer studies (Santos *et al.*, 2018; Keijzer *et al.*, 2019) reported a moderate reproducibility: variabilities up to 1 m/s were observed, mainly due to measurement inaccuracies such as a limited SNR and shear wave tracking length. Keijzer et al. (Keijzer *et al.*, 2019) suggested to improve measurement precision by averaging wave speeds over 10 heartbeats and multiple M-mode line analyses per recording.

Most of the presented work in this review has been performed with research systems or clinical systems that have been adapted for research purposes. For ARF-based SWE, several commercial elastography functions are available from different vendors (e.g. Shear Wave Elastography from SuperSonic Imagine, Virtual Touch™ quantification from Philips/Siemens (Sigrist *et al.*, 2017; Barr *et al.*, 2015)), but these are primarily used for liver and breast tissue and are not optimized yet for cardiac applications. For natural SWE, tissue Doppler imaging (TDI) applications on current clinical scanners can be used. Indeed, Pislaru et al. (Pislaru *et al.*, 2017) reported a frame rate of 350-460 Hz on the GE Vivid E9 and Philips iE33 scanner. This can even be elevated to 400-700 Hz on the Philips iE33 system (Strachinaru *et al.*, 2017). Recently, Canon Medical Systems provides Shear Wave Dispersion Imaging for determining tissue's viscoelastic properties in case of fibrotic liver disease (Sugimoto *et al.*, 2020). It can be expected that with time, high-end commercial systems and corresponding software can be made ready for cardiac SWE – natural as well as ARF-based – while evidence of the additional clinical information is building up.

Future perspectives

Best practices in cardiac shear wave elastography

As the number of clinical studies on cardiac SWE is growing, the need for consistent data collection and reporting is urgent, and we formulate some recommendations that may improve SWE accuracy and facilitate comparison of SWE results between studies. With the currently available 2D SWE technology, shear waves are typically tracked in the IVS which is located not too deep nor too shallow for shear wave generation/tracking. The echocardiographic views are limited to PLAX or PSAX for ARF-based SWE, because a quasi-orthogonal relationship between ultrasound beam and cardiac wall is required for inducing transversal wave motion. On the other hand, for natural shear waves, PLAX or AP4C view can be used. It should however be noted that each view tracks a different component of tissue motion and thus potentially a different wave mode (Keijzer *et al.*, 2020b). Depending on the technological advancements, more echocardiographic views/regions might be possible in the near future.

A variety of SWE-metrics have been reported in literature (illustrated in Table 3 and Table 4). We strongly discourage reporting a shear or Young's modulus through the use of equations (1) and/or (3), since this is associated with stringent assumptions concerning mechanical properties which do not hold for the myocardium (i.e. linear elasticity, isotropy and bulk size). Figure 10 summarizes our recommendations for data reporting in cardiac SWE in clinical practice. Ideally, future research should clearly report the propagation speed of the traveling wave in the time domain together with the main excited frequency. As it is unclear up to now what type of tissue motion (velocity/acceleration) should best be used to determine wave speed, we suggest to report propagation speeds based on both tissue velocity and acceleration to enable comparison between future studies. Furthermore, it is recommended to also report (Figure 10): (i) system-dependent factors which have a non-negligible effect on SWE results but are inherent to the available SWE modality, (ii) technical settings on which operators do have their say and (iii) population characteristics describing mechanical and biological variations. Concerning technical settings, next to echocardiographic view and cardiac region as discussed before, the M-line for wave speed estimation should be positioned in the middle of the cardiac wall parallel to the border (i.e. along the assumed propagation direction). We suggest to repeat this M-line measurement multiple times for multiple SWE acquisitions and to report the median speed together with its interquartile range (Santos *et al.*, 2018; Keijzer *et al.*, 2019). A more advanced material characterization can be obtained from SWE by studying the wave's frequency behavior (dispersion) or multiple echocardiographic views (anisotropy). However, we note that advanced material characterization can be challenging and is often associated with more variable results in low SNR data which can increase the complexity of inter-study comparisons; as such, we recommend including the group SWS measurements as well in these studies. If the resolution of the imaging system is high enough, transmural wave speed variations can also be studied to investigate the myocardial anisotropy, especially in PSAX (see Figure 8). As the wave propagation direction is unknown for natural SWE, 3D imaging will offer additional insights for advancing material characterization.

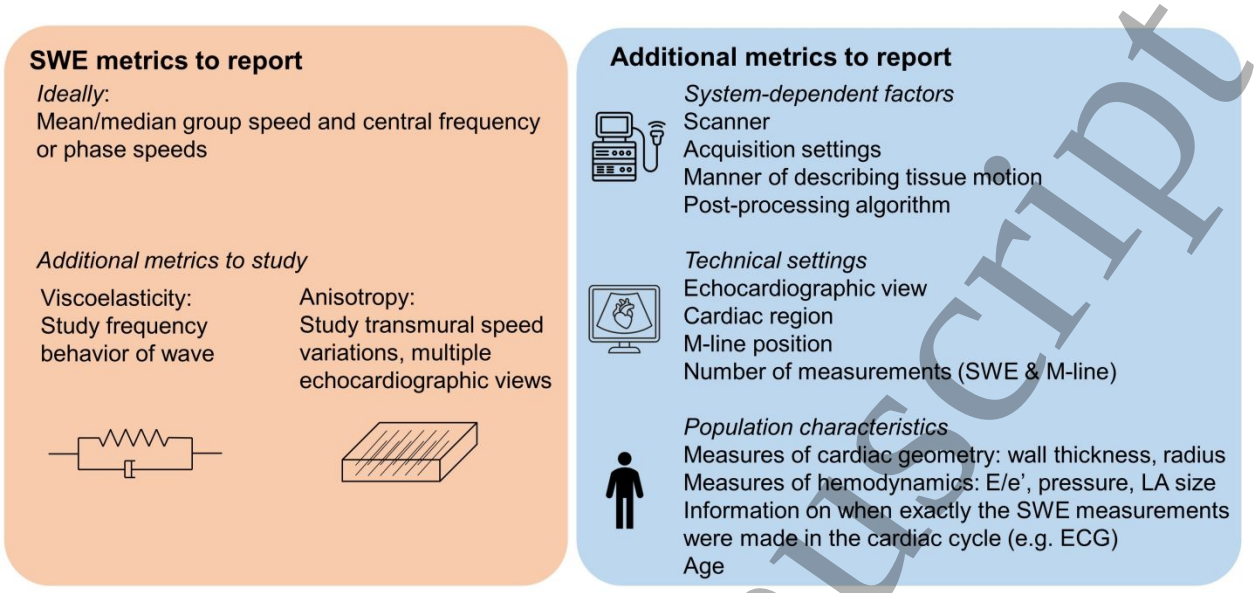

Figure 10 – Recommendations for standardized data reporting based on the currently available SWE technology in the clinics.

Technical and mechanical challenges to overcome

Even though multiple clinical studies have successfully reported results of transthoracic SWE, the technique still faces many challenges of both a technical and mechanical nature. Indeed, the feasibility of transthoracic ARF-based SWE – especially in systole – is generally lower than for natural SWE due to difficulties to transmit a sufficient amount of energy into the cardiac wall for shear wave excitation and to consequently track the generated wave in an acoustically safe manner. This is partly due to location of the heart which is encased by ribs and surrounded by lung tissue limiting the acoustic accessibility. An external vibrator might overcome the limitations of penetration depth, but is associated with other issues such as shear wave speed estimation biases due to misalignment of the measurement plane and the excitation source but also coupling uncertainties of the vibration energy into the myocardium. The magnitude of particle motion for natural SWE is in general higher than for ARF-based SWE (tens of mm/s instead of a few mm/s in Figure 9), however the wave speed might be less accurately tracked because of a larger spatial wavelength (a few cm vs. a few mm in Figure 9) within the limited field-of-view (3-4 cm). Additionally, the technical settings of the used elastography mode on the ultrasound scanner (e.g. temporal and spatial characteristics of the ARF, tissue motion estimation algorithm, shear wave speed estimation algorithm, etc.) will also affect the resulting wave speed. A clear communication of the device manufacturer to the sonographers and physicians is necessary to better understand what the system is reporting. We have formulated some guidelines on standardization of SWE data collection and reporting, but it is clear that a dedicated committee endorsed by the leading echography/cardiology societies needs to set these criteria as has been done for the staging of liver fibrosis (Quantitative Imaging Biomarker Alliance by the Radiological Society of North America (Palmeri *et al.*, 2021)) and cardiac speckle tracking echocardiography (Voigt *et al.*, 2015).

This paper focused on mechanical factors interfering with cardiac SWE. However, the sensitivity of the SWE technique to each considered mechanical factor remains unclear: is SWE more

sensitive to changes in myocardial mechanical properties than to, for example, changes in hemodynamics? And is this different for ARF-based and natural SWE? Furthermore, the arrival of 3D SWE might further improve our understanding of both types of SWE, especially for natural SWE as the spatial and temporal characteristics of the wave excitation source are unknown. It should also be noted that shear wave measurements provide only a local measurement of stiffness, assessed within the size of the field of view, and it should be further investigated how this relates to global stiffness changes, as reflected by an altered end-diastolic pressure-volume relationship.

Conclusion

Ultrasound-based SWE has a tremendous potential for non-invasive characterization of the active and passive stiffness of the heart. The number of clinical studies demonstrating the discriminative power of shear wave speed for cardiac pathology is growing. However, one should be aware that mechanical factors, next to pathology, affect wave speed estimation. With this paper, we aim to contribute to a better conceptual understanding of shear wave physics and, consequently, a deeper insight for a correct interpretation of findings.

Acknowledgements

This work was supported by the Research Foundation Flanders (FWO, Brussels, Belgium) under grant 1211620N to Annette Caenen.

Kathryn R. Nightingale has intellectual property related to radiation force-based imaging technologies that has been licensed to Siemens, Samsung and MicroElastic Ultrasound Systems. The other authors declare that they have no conflict of interest.

Appendix A: Lamb waves in cardiac SWE

The cardiac wall is typically approximated as a fluid-loaded (visco)elastic plate, for which the Lamb wave theory is manipulated to better understand the geometrical (and viscoelastic) effect on cardiac shear wave propagation (Nguyen *et al.*, 2011; Nenadic *et al.*, 2011; Pislaru *et al.*, 2014b; Urban *et al.*, 2013; Kanai, 2005; Keijzer *et al.*, 2020b). When viscoelasticity is included, a Voigt model is commonly used to describe the rheological behavior. This material model assumes a viscous component represented by a dashpot (with viscosity η) in parallel with the elastic component (spring with spring constant μ). To better understand the effect of geometry and viscoelasticity on wave propagation, we plotted the theoretical phase speed characteristics of Lamb waves for a representative elastic and viscoelastic myocardial model in diastole and systole in Figure A11a, in comparison to that of a bulk medium with the same material parameters. The effect of geometry can be derived by comparing the phase speed characteristics of a bulk medium to that of the plates for an elastic material: the phase speed is independent of frequency for bulk media (1.3 m/s in diastole and 4.8 m/s in systole); whereas the phase speeds in plates increase as a function of frequency until they reach a plateau-value (i.e. the plate wave speed, which is about 95 % of the bulk shear wave speed (Rose, 2014)). The effect of viscoelasticity is also demonstrated in Figure A11a, and shows for phase speed an increasing trend as a function of frequency independent of the considered geometry. It should be noted that geometry, viscoelasticity or a combination of the two can result in wave dispersion, but is dependent on the excitation properties (e.g. bandwidth, central frequency) if dispersion is observed. For example, when considering a traveling mechanical wave with a frequency content between 200-400 Hz, Figure A11a shows a frequency-dependent wave speed in systole for an elastic plate of 10 mm, but not for an elastic plate of 15 mm. Figure A11a also demonstrates that low frequency excitations such as natural waves after valve closure are more sensitive to thickness variations: the phase speed can increase 24 % (peak frequency of 40 Hz for MVC (Vos *et al.*, 2017)) in diastole and 40 % in systole (peak frequency of 80 Hz for AVC (Vos *et al.*, 2017)) when myocardial thickness changes from 10 to 15 mm.

Some cardiac SWE studies (Kanai, 2005; Urban *et al.*, 2013; Nenadic *et al.*, 2018; Pislaru *et al.*, 2014b) have set one step further in post-processing the SWE results by reporting elasticity and viscosity values using the Lamb wave model, as summarized in Table A5. The process to estimate elasticity and viscosity values is as follows. First, the frequency-dependent behavior of the studied mechanical wave is investigated by (i) performing multiple wave speed measurements while varying the frequency of the mechanical actuator (Pislaru *et al.*, 2014b; Urban *et al.*, 2013) or by (ii) applying a fast Fourier transform (FFT) on the temporal wave data to analyze the frequency content of the mechanical wave (Deffieux *et al.*, 2009; Couade *et al.*, 2010). Both cases will give the phase speed characteristics as a function of frequency, of which examples are shown for two types of shear wave excitation in Figure A11b. Second, elasticity and viscosity values are obtained by fitting the theoretical Lamb wave model to the measured phase speed characteristics. LV phantom studies (Caenen *et al.*, 2017; Sabbadini *et al.*, 2021) have shown that the elasticity results based on the phase speed will better approach the true stiffness than those based on the group speed (deviations up to +12 % vs. -67 %). However, it should be noted that this Lamb wave fitting comes with several assumptions such as plate geometry, smooth walls, and isotropy which

do not hold for the cardiac wall. Furthermore, frequency analyses in *in vivo* cardiac SWE are sparsely reported in literature (Vos *et al.*, 2017; Kanai, 2005) because of the non-suitability of mechanical actuators *in vivo* (resulting in a broadband excitation) and the low resolution in combination with low SNR for an accurate FFT. Furthermore, frequency analysis on natural waves do not allow to get a complete picture of the frequency behavior of the tissue of interest because of their relatively narrow bandwidth <150Hz (Vos *et al.*, 2017; Keijzer *et al.*, 2019).

All reported elasticity and viscosity values in Table A5 are in the same range, except for the systolic elasticity and viscosity reported by Kanai et al. (Kanai, 2005) ($\mu_1 = 30\ kPa$ and $\mu_2 = 70 - 400\ Pa \cdot s$), which is larger than the elasticity and viscosity reported by the other studies in Table A5. This might be due to a difference in investigated region (septum vs. free wall), a different view showing different wave types (Keijzer *et al.*, 2020b) or a variable accuracy in the Lamb wave analysis when the frequency of the wave excitation alters.

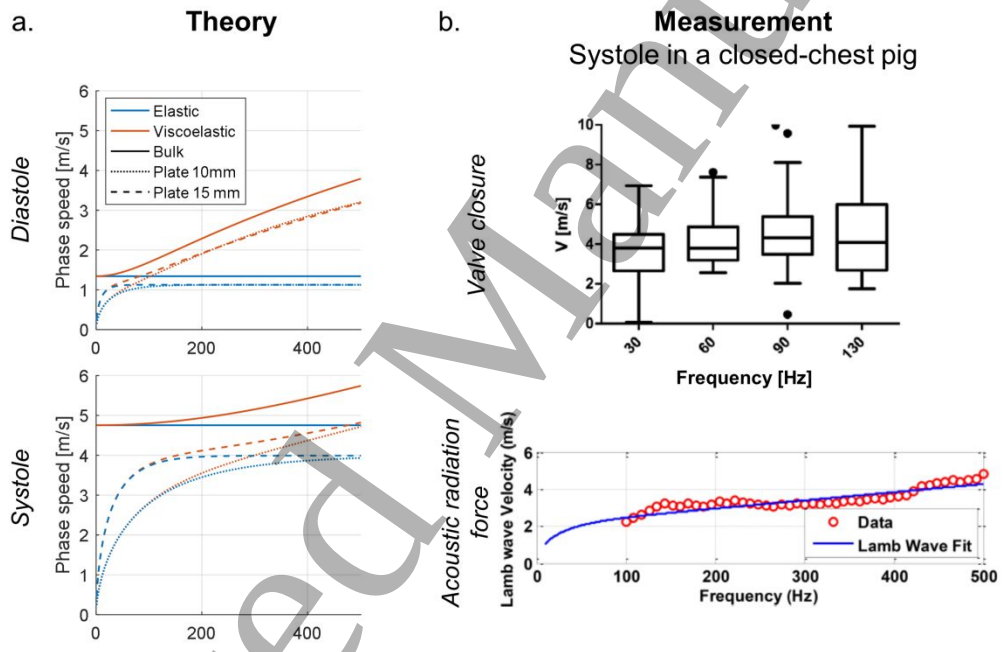

Figure A11 – Effect of geometry and viscoelasticity on shear wave properties. (a) Theoretical predictions of the phase speed variations in a bulk medium and plate (with a thickness of 10 mm and 15 mm), when assuming an elastic and viscoelastic medium (Voigt model). The material parameters are $\mu = 1.8\ kPa$ (and $\eta = 2.7\ Pa \cdot s$) in diastole; and $\mu = 22.6\ kPa$ (and $\eta = 5.9\ Pa \cdot s$) in systole – as reported by Pislaru et al. (Pislaru et al., 2014b). Note that the phase speed characteristics of one mode (antisymmetric zero order mode) – expected dominant mode in cardiac SWE – are shown for a fluid-loaded plate. (b) Measured shear wave spectra in a closed-chest pig in systole: group velocities after aortic valve closure (Vos et al., 2017) (upper panel) and phase velocities in systole after acoustic radiation force application (Nenadic et al., 2018) (lower panel). Adapted with permission from Vos et al. (Vos et al., 2017) and Nenadic et al. (Nenadic et al., 2018).

Table A5 – Reported viscoelastic properties in cardiac SWE when assuming a plate-like myocardium with its viscoelastic material properties obeying a Voigt model. Diastolic values in natural SWE corresponds to wave analysis after mitral valve closure; whereas systolic values are obtained for wave analysis after aortic valve closure. (VC: valve closure, MS: mechanical stimulation, ARF: acoustic radiation force, IVS: interventricular septum, LVFW: left ventricular free wall, NR: not reported)

Study	Excit	Region	Species	Diastole	Systole

(ref #)	ation			Elasticity μ [kPa]	Viscosity η [Pa·s]	Elasticity μ [kPa]	Viscosity η [Pa·s]
(Kanai, 2005)	VC	IVS	Human (n=5)	NR	NR	30 kPa	70-400 Pa·s
(Urban *et al.*, 2013)	MS	LVFW	Open-chest pig (n=8)	1.81±0.8 kPa	2.7±0.56 Pa·s	21.14±7.72 kPa	4.16±4.32 Pa·s
(Pislaru *et al.*, 2014b)	MS	LVFW	Open-chest pig (n=10)	1.8±0.8 kPa	2.7±0.9 Pa·s	22.6±6 kPa	5.9±4.7 Pa·s
(Nenadic *et al.*, 2018)	ARF	LVFW	Open-chest pig (n=1)	2.24±0.54 kPa	3.36±0.5 Pa·s	12.44±1.3 kPa	3.99±1.19 Pa·s
(Nenadic *et al.*, 2018)	ARF	LVFW	Pig (n=1)	5.1 kPa	3.2 Pa·s	19.1 kPa	6.8 Pa·s

References

Barr R G, Nakashima K, Amy D, Cosgrove D, Farrokh A, Schafer F, Bamber J C, Castera L, Choi B I, Chou Y H, Dietrich C F, Ding H, Ferraioli G, Filice C, Friedrich-Rust M, Hall T J, Nightingale K R, Palmeri M L, Shiina T, Suzuki S, Sporea I, Wilson S and Kudo M 2015 WFUMB guidelines and recommendations for clinical use of ultrasound elastography: Part 2: breast *Ultrasound Med Biol* **41** 1148-60

Bercoff J, Tanter M, Muller M and Fink M 2004 The Role of Viscosity in the Impulse Diffraction Field of Elastic Waves Induced by the Acoustic Radiation Force *IEEE Trans Ultrason Ferroelectr Freq Control* **51** 1523-36

Bezy S, Cvijic M, Petrescu A, Orlowska M, Santos P, Duchenne J, Chakraborty B, Pedrosa J, D'Hooge J and Voigt J U 2020a Shear wave propagation velocity after aortic valve closure could be a novel parameter for myocardial contractility *European Heart Journal - Cardiovascular Imaging* **21**

Bezy S, Duchenne J, Orlowska M, Wouters L, Caenen A, Keijzer L B H, Cvijic M, D'Hooge J and Voigt J U 2020b The behaviour of natural shear waves under different loading conditions *European Heart Journal* **41**

Bezy S, Petrescu A, Cvijic M, Orlowska M, Santos P, Werner A E, Duchenne J, Voigt J U and D'Hooge J 2020c Determinants of the propagation velocity of natural shear waves in cardiac shear wave elastography. In: *IEEE International Ultrasound Symposium,* (Las Vegas, NV, USA

Bouchard R, Hsu D, Wolf P and Trahey G 2009 In Vivo Cardiac Acoustic-Radiation-Force-Driven Shear Wave Velocimetry *Ultrason Imaging* **31** 201-13

Brekke B, Nilsen L C, Lund J, Torp H, Bjastad T, Amundsen B H, Stoylen A and Aase S A 2014 Ultra-high frame rate tissue Doppler imaging *Ultrasound in medicine & biology* **40** 222-31

Caenen A, Pernot M, Peirlinck M, Mertens L, Swillens A and Segers P 2018 An in silico framework to analyze the anisotropic shear wave mechanics in cardiac shear wave elastography *Physics in medicine and biology* **63**

Caenen A, Pernot M, Shcherbakova D A, Mertens L, Kersemans M, Segers P and Swillens A 2017 Investigating Shear Wave Physics in a Generic Pediatric Left Ventricular Model via In Vitro Experiments and Finite Element Simulations *IEEE Trans Ultrason Ferroelectr Freq Control* **64** 349-61

Catheline S and Benech N 2015 Longitudinal shear wave and transverse dilatational wave in solids *J Acoust Soc Am* **137** 200-5

Catheline S, Wu F and Fink M 1999 A solution to diffraction biases in sonoelasticity: The acoustic impulse technique *J Acoust Soc Am* **105** 2941-50

Cobbold R S C 2002 *Foundations of Biomedical Ultrasound*: Oxford University Press)

Couade M, Pernot M, Messas E, Bel A, Ba M, Hagege A, Fink M and Tanter M 2011 In vivo quantitative mapping of myocardial stiffening and transmural anisotropy during the cardiac cycle *IEEE Trans Med Imaging* **30** 295-305

Couade M, Pernot M, Prada C, Messas E, Emmerich J, Bruneval P, Criton A, Fink M and Tanter M 2010 Quantitative assessment of arterial wall biomechanical properties using shear wave imaging *Ultrasound Med Biol* **36** 1662-76

Cvijic M, Bezy S, Petrescu A, Santos P, Orlowska M, Chakraborty B, Duchenne J, Pedrosa J, Vanassche T, D'Hooge J and Voigt J U 2020 Interplay of cardiac remodelling and myocardial stiffness in hypertensive heart disease: a shear wave imaging study using high-frame rate echocardiography *Eur Heart J Cardiovasc Imaging* **21** 664-72

Deffieux T, Montaldo G, Tanter M and Fink M 2009 Shear wave spectroscopy for in vivo quantification of human soft tissues visco-elasticity *IEEE Trans Med Imaging* **28** 313-22

Deng Y, Rouze N C, Palmeri M L and Nightingale K R 2017 Ultrasonic Shear Wave Elasticity Imaging (SWEI) Sequencing and Data Processing Using a Verasonics Research Scanner *IEEE Trans Ultrason Ferroelectr Freq Control* 1-

Elgeti T, Knebel F, Hättasch R, Hamm B, Braun J and Sack I 2014 Shear-wave amplitudes measured with cardiac MR elastography for diagnosis of diastolic dysfunction *Radiology* **271** 681-7

Elgeti T and Sack I 2014 Magnetic Resonance Elastography of the Heart *Current Cardiovascular Imaging Reports* **7**

Ferraioli G, Filice C, Castera L, Choi B I, Sporea I, Wilson S R, Cosgrove D, Dietrich C F, Amy D, Bamber J C, Barr R, Chou Y H, Ding H, Farrokh A, Friedrich-Rust M, Hall T J, Nakashima K, Nightingale K R, Palmeri M L, Schafer F, Shiina T, Suzuki S and Kudo M 2015 WFUMB guidelines and recommendations for clinical use of ultrasound elastography: Part 3: liver *Ultrasound Med Biol* **41** 1161-79

Fung Y C 1993 *Biomechanics - Mechanical Properties of Living Tissues*

Gao L, Parker K J, Lerner R M and Levinson S F 1996 Imaging of the elastic properties of tissue - A review *Ultrasound Med Biol* **22** 959-77

Greenleaf J F, Fatemi M and Insana M 2003 Selected methods for imaging elastic properties of biological tissues *Annu Rev Biomed Eng* **5** 57-78

Guimarães C F, Gasperini L, Marques A P and Reis R L 2020 The stiffness of living tissues and its implications for tissue engineering *Nature Reviews Materials* **5** 351-70

Hollender P, Bradway D, Wolf P, Goswami R and Trahey G 2013 Intracardiac acoustic radiation force impulse (ARFI) and shear wave imaging in pigs with focal infarctions *IEEE Trans Ultrason Ferroelectr Freq Control* **60** 1669-82

Hollender P J, Wolf P D, Goswami R and Trahey G E 2012 Intracardiac echocardiography measurement of dynamic myocardial stiffness with shear wave velocimetry *Ultrasound Med Biol* **38** 1271-83

Kanai H 2005 Propagation of spontaneously actuated pulsive vibration in human heart wall and in vivo viscoelasticity estimation. *IEEE Trans Ultrason Ferroelectr Freq Control* **52** 1931-42

Kasai C, Namekawa K, Koyano A and Omoto R 1985 Real-Time Two-Dimensional Blood Flow Imaging Using an Autocorrelation Technique *IEEE Trans Sonics Ultrasonics* **SU-32** 458-64

Keijzer L B H, Bosch J G, Verweij M D, De Jong N and Vos H J *IEEE International Ultrasound Symposium, (Washington DC, USA, 2018),* vol. Series*)* pp 1-4

Keijzer L B H, Caenen A, Voorneveld J, Strachinaru M, Bowen D J, van de Wouw J, Sorop O, Merkus D, Duncker D J, van der Steen A F W, de Jong N, Bosch J G and Vos H J 2020a A direct comparison of natural and acoustic-radiation-force-induced cardiac mechanical waves *Sci Rep* **10** 18431

Keijzer L B H, Strachinaru M, Bowen D J, Caenen A, Van der Steen A F W, Verweij M D, De Jong N, Bosch J G and Vos H J 2020b Parasternal versus Apical View in Cardiac Natural Mechanical Wave Speed Measurements *IEEE Trans Ultrason Ferroelectr Freq Control* **67** 1590-602

Keijzer L B H, Strachinaru M, Bowen D J, Geleijnse M L, van der Steen A F W, Bosch J G, de Jong N and Vos H J 2019 Reproducibility of Natural Shear Wave Elastography Measurements *Ultrasound Med Biol* **45** 3172-85

Knight A E, Trutna C A, Rouze N C, Hobson-Webb L D, Caenen A, Jin F Q, Palmeri M L and Nightingale K R 2021 Full Characterization of in vivo Muscle as an Elastic, Incompressible, Transversely Isotropic Material using Ultrasonic Rotational 3D Shear Wave Elasticity Imaging *IEEE Trans Med Imaging* **PP**

Kwiecinski W, Bessiere F, Colas E C, N'Djin W A, Tanter M, Lafon C and Pernot M 2015 Cardiac shear-wave elastography using a transesophageal transducer: application to the mapping of thermal lesions in ultrasound transesophageal cardiac ablation *Phys Med Biol* **60** 7829-46

Lee W N, Larrat B, Pernot M and Tanter M 2012a Ultrasound elastic tensor imaging: comparison with MR diffusion tensor imaging in the myocardium *Phys Med Biol* **57** 5075-95

Lee W N, Pernot M, Couade M, Messas E, Bruneval P, Bel A, Hagege A A, Fink M and Tanter M 2012b Mapping myocardial fiber orientation using echocardiography-based shear wave imaging *IEEE Trans Med Imaging* **31** 554-62

Mariappan Y K, Glaser K J and Ehman R L 2010 Magnetic resonance elastography: a review *Clin Anat* **23** 497-511

Montaldo G, Tanter M, Bercoff J, Benech N and Fink M 2009 Coherent Plane-Wave Compounding for Very High Frame Rate Ultrasonography and Transient Elastography *IEEE Trans Ultrason Ferroelectr Freq Control* **56** 489-506

Nenadic I Z, Urban M W, Mitchell S A and Greenleaf J F 2011 Lamb wave dispersion ultrasound vibrometry (LDUV) method for quantifying mechanical properties of viscoelastic solids *Phys Med Biol* **56** 2245-64

Nenadic I Z, Urban M W, Pislaru C, Escobar D, Vasconcelos L and Greenleaf J F 2018 In Vivo Open- and Closed-chest Measurements of Left-Ventricular Myocardial Viscoelasticity using Lamb wave Dispersion Ultrasound Vibrometry (LDUV): A Feasibility Study *Biomed Phys Eng Express* **4**

Nguyen T-M, Couade M, Bercoff J and Tanter M 2011 Assessment of Viscous and Elastic Properties of Sub-Wavelength Layered Soft Tissues Using Shear Wave Spectroscopy: Theoretical Framework and In Vitro Experimental Validation *IEEE Trans Ultrason Ferroelectr Freq Control* **58** 2305-15

Nightingale K R, Palmeri M L, Nightingale R W and Trahey G E 2001 On the feasibility of remote palpation using acoustic radiation force *J Acoust Soc Am* **110** 625-34

Nightingale K R, Rouze N C, Rosenzweig S J, Wang M H, Abdelmalek M F, Guy C D and Palmeri M L 2015 Derivation and analysis of viscoelastic properties in human liver: impact of frequency on fibrosis and steatosis staging *IEEE Trans Ultrason Ferroelectr Freq Control* **62** 165-75

Olson T R and Pawlina W 2008 *A.D.A.M. Student Atlas of Anatomy*

Ophir J, Céspedes H, Ponnekanti H, Yazdi Y and Li X 1991 Elastography: A quantitative method for imaging the elasticity of biological tissues *Ultrason Imaging* **13** 111-34

Palmeri M L, Milkowski A, Barr R, Carson P, Couade M, Chen J, Chen S, Dhyani M, Ehman R, Garra B, Gee A, Guenette G, Hah Z, Lynch T, Macdonald M, Managuli R, Miette V, Nightingale K R, Obuchowski N, Rouze N C, Morris D C, Fielding S, Deng Y, Chan D, Choudhury K, Yang S, Samir A E, Shamdasani V, Urban M, Wear K, Xie H, Ozturk A, Qiang B, Song P, McAleavey S, Rosenzweig S, Wang M, Okamura Y, McLaughlin G, Chen Y, Napolitano D, Carlson L, Erpelding T and Hall T J 2021 Radiological Society of North America/Quantitative Imaging Biomarker Alliance Shear Wave Speed Bias Quantification in Elastic and Viscoelastic Phantoms *J Ultrasound Med* **40** 569-81

Papadacci C, Finel V, Villemain O, Tanter M and Pernot M 2020 4D Ultrafast Ultrasound Imaging of Naturally Occurring Shear Waves in the Human Heart *IEEE Transactions on Medical Imaging* **39** 4436-44

Parker K J, Ormachea J and Hah Z 2018 Group versus Phase Velocity of Shear Waves in Soft Tissues *Ultrason Imaging* **40** 343-56

Pernot M, Couade M, Mateo P, Crozatier B, Fischmeister R and Tanter M 2011 Real-time assessment of myocardial contractility using shear wave imaging *J Am Coll Cardiol* **58** 65-72

Pernot M, Lee W-N, Bel A, Mateo P, Couade M, Tanter M, Crozatier B and Messas E 2016 Shear wave imaging of passive diastolic myocardial stiffness: stunned vs infarcted myocardium *JACC Cardiovasc Imaging* **9** 1023-30

Pernot M and Villemain O 2019 In the Heart of Stiffness: Are Natural Heart Vibrations Reliable Enough to Assess Myocardial Stiffness, The New Holy Grail in Echocardiography? *JACC Cardiovasc Imaging* **12** 2399-401

Petrescu A, Bezy S, Cvijic M, Santos P, Orlowska M, Duchenne J, Pedrosa J, Van Keer J M, Verbeken E, von Bardeleben S, Droogne W, Bogaert J, Van Cleemput J, D'Hooge J and Voigt J U 2020 Shear Wave

Elastography Using High-Frame-Rate Imaging in the Follow-Up of Heart Transplantation Recipients *JACC Cardiovasc Imaging* **13** 2304-13

Petrescu A, Santos P, Orlowska M, Pedrosa J, Bezy S, Chakraborty B, Cvijic M, Dobrovie M, Delforge M, D'Hooge J and Voigt J U 2019 Velocities of Naturally Occurring Myocardial Shear Waves Increase With Age and in Cardiac Amyloidosis *JACC Cardiovasc Imaging* **12** 2389-98

Pislaru C, Alashry M M, Thaden J J, Pellikka P A, Enriquez-Sarano M and Pislaru S V 2017 Intrinsic Wave Propagation of Myocardial Stretch, A New Tool to Evaluate Myocardial Stiffness: A Pilot Study in Patients with Aortic Stenosis and Mitral Regurgitation *J Am Soc Echocardiogr* **30** 1070-80

Pislaru C, Pellikka P A and Pislaru S V 2014a Wave propagation of myocardial stretch: correlation with myocardial stiffness *Basic research in cardiology* **109** 438

Pislaru C, Urban M W, Pislaru S V, Kinnick R R and Greenleaf J F 2014b Viscoelastic properties of normal and infarcted myocardium measured by a multifrequency shear wave method: comparison with pressure-segment length method *Ultrasound Med Biol* **40** 1785-95

Rose J L 2014 *Ultrasonic guided waves in solid media* (New York: Cambridge University Press)

Rouze N C, Wang M H, Palmeri M L and Nightingale K R 2013 Finite element modeling of impulsive excitation and shear wave propagation in an incompressible, transversely isotropic medium *J Biomech* **46** 2761-8

Sabbadini A, Caenen A, Keijzer L B H, van Neer P, Vos H J, de Jong N and Verweij M D 2021 Tapering of the interventricular septum can affect ultrasound shear wave elastography: An in vitro and in silico study *J Acoust Soc Am* **150** 428

Salles S, Espeland T, Molares A, Aase S A, Hammer T A, Støylen A, Aakhus S, Lovstakken L and Torp H 2020 3D Myocardial Mechanical Wave Measurements *JACC: Cardiovascular Imaging*

Salles S, Lovstakken L, Aase S A, Bjastad T G and Torp H 2019 Clutter Filter Wave Imaging *IEEE Trans Ultrason Ferroelectr Freq Control* **66** 1444-52

Sandrin L, Catheline S, Tanter M, Hennequin X and Fink M 1999 Time-resolved pulsed elastography with ultrafast ultrasonic imaging *Ultrason Imaging* **21** 259-72

Santos P, Petrescu A, Pedrosa J, Orlowska M, Komini V, Voigt J-U and D'hooge J 2018 Natural shear wave imaging in the human heart: normal values, feasibility and reproducibility *IEEE Trans Ultrason Ferroelectr Freq Control* **66** 442-52

Sarvazyan A P, Rudenko O V, Swanson S D, Fowlkes J B and Emelianov S Y 1998 Shear Wave Elasticity Imaging: a New Ultrasonics Technology of Medical Diagnostics *Ultrasound Med Biol* **24** 1419-35

Sarvazyan A P, Urban M W and Greenleaf J F 2013 Acoustic Waves in Medical Imaging and Diagnostics *Ultrasound in Medicine & Biology* **39** 1133-46

Sigrist R M S, Liau J, Kaffas A E, Chammas M C and Willmann J K 2017 Ultrasound Elastography: Review of Techniques and Clinical Applications *Theranostics* **7** 1303-29

Song P, Bi X, Mellema D C, Manduca A, Urban M W, Greenleaf J F and Chen S 2016 Quantitative Assessment of Left Ventricular Diastolic Stiffness Using Cardiac Shear Wave Elastography: A Pilot Study *J Ultrasound Med* **35** 1419-27

Song P, Urban M W, Chen S, Manduca A, Zhao H, Nenadic I, Pislaru S V, Pislaru C and Greenleaf J F *IEEE International Ultrasonics Symposium,2014),* vol. Series*)*: IEEE) pp 109-12

Song P, Zhao H, Urban M W, Manduca A, Pislaru S V, Kinnick R R, Pislaru C and Chen S 2013 Improved shear wave motion detection using pulse-inversion harmonic imaging with phased array transducer *IEEE Trans Med Imaging* **32** 2299-310

Strachinaru M, Bosch J G, van Dalen B M, van Gils L, van der Steen A F W, de Jong N, Geleijnse M L and Vos H J 2017 Cardiac Shear Wave Elastography Using a Clinical Ultrasound System *Ultrasound Med Biol* **43** 1596-606

Strachinaru M, Bosch J G, van Gils L, van Dalen B M, Schinkel A F L, van der Steen A F W, de Jong N, Michels M, Vos H J and Geleijnse M L 2019a Naturally Occurring Shear Waves in Healthy Volunteers and Hypertrophic Cardiomyopathy Patients *Ultrasound Med Biol* **45** 1977-86

Strachinaru M, Geleijnse M L, de Jong N, van den Bosch A, Michels M, Schinkel A F L, van der Steen A F W, Bosch J G and Vos H J 2019b Myocardial Stretch Post-atrial Contraction in Healthy Volunteers and Hypertrophic Cardiomyopathy Patients *Ultrasound Med Biol* **45** 1987-98

Sugimoto K, Moriyasu F, Oshiro H, Takeuchi H, Yoshimasu Y, Kasai Y and Itoi T 2020 Clinical utilization of shear wave dispersion imaging in diffuse liver disease *Ultrasonography* **39** 3-10

Trutna C A, Rouze N C, Palmeri M L and Nightingale K R 2020 Measurement of Viscoelastic Material Model Parameters Using Fractional Derivative Group Shear Wave Speeds in Simulation and Phantom Data *IEEE Trans Ultrason Ferroelectr Freq Control* **67** 286-95

Tzschatzsch H, Elgeti T, Rettig K, Kargel C, Klaua R, Schultz M, Braun J and Sack I 2012 In Vivo time harmonic elastography of the human heart *Ultrasound Med Biol* **38** 214-22

Urban M W, Pislaru C, Nenadic I Z, Kinnick R R and Greenleaf J F 2013 Measurement of viscoelastic properties of in vivo swine myocardium using lamb wave dispersion ultrasound vibrometry (LDUV) *IEEE Trans Med Imaging* **32** 247-61

Vejdani-Jahromi M, Freedman J, Kim Y-J, Trahey G E and Wolf P D 2018 Assessment of Diastolic Function Using Ultrasound Elastography *Ultrasound Med Biol* **44** 551-61

Vejdani-Jahromi M, Freedman J, Nagle M, Kim Y-J, Trahey G E and Wolf P D 2017 Quantifying Myocardial Contractility Changes Using Ultrasound-Based Shear Wave Elastography *J Am Soc Echocardiogr* **30** 90-6

Vejdani-Jahromi M, Nagle M, Jiang Y, Trahey G and Wolf P 2016 A comparison of acoustic radiation force derived indices of cardiac function in the Langendorff perfused rabbit heart *IEEE Trans Ultrason Ferroelectr Freq Control* **63** 1288-95

Vejdani-Jahromi M, Nagle M, Trahey G E and Wolf P D 2015 Ultrasound shear wave elasticity imaging quantifies coronary perfusion pressure effect on cardiac compliance *IEEE Trans Med Imaging* **34** 465-73

Villemain O, Baranger J, Friedberg M K, Papadacci C, Dizeux A, Messas E, Tanter M, Pernot M and Mertens L 2020 Ultrafast Ultrasound Imaging in Pediatric and Adult Cardiology: Techniques, Applications, and Perspectives *JACC Cardiovasc Imaging* **13** 1771-91

Villemain O, Correia M, Mousseaux E, Baranger J, Zarka S, Podetti I, Soulat G, Damy T, Hagège A and Tanter M 2018 Myocardial Stiffness Evaluation Using Noninvasive Shear Wave Imaging in Healthy and Hypertrophic Cardiomyopathic Adults *JACC: Cardiovascular Imaging* **12** 1135-45

Voigt J U, Pedrizzetti G, Lysyansky P, Marwick T H, Houle H, Baumann R, Pedri S, Ito Y, Abe Y, Metz S, Song J H, Hamilton J, Sengupta P P, Kolias T J, d'Hooge J, Aurigemma G P, Thomas J D and Badano L P 2015 Definitions for a common standard for 2D speckle tracking echocardiography: consensus document of the EACVI/ASE/Industry Task Force to standardize deformation imaging *Eur Heart J Cardiovasc Imaging* **16** 1-11

Vos H J, van Dalen B M, Heinonen I, Bosch J G, Sorop O, Duncker D J, van der Steen A F and de Jong N 2017 Cardiac Shear Wave Velocity Detection in the Porcine Heart *Ultrasound Med Biol* **43** 753-64

Wang M, Byram B, Palmeri M, Rouze N and Nightingale K 2013 Imaging transverse isotropic properties of muscle by monitoring acoustic radiation force induced shear waves using a 2-D matrix ultrasound array *IEEE Trans Med Imaging* **32** 1671-84